Title
FILAMENTARY NIOBIUM-TIN SUPERCONDUCTORS FABRICATED BY A POWDER METALLURGY APPROACH

Author
Hemachalam, Kanithl.

Publication Date
1976-02-01

FILAMENTARY NIOBIUM-TIN SUPERCONDUCTORS FABRICATED BY A POWDER METALLURGY APPROACH

Kanithi Hemachalam
(D. Eng. Thesis)

February 1976

Prepared for the U. S. Energy Research and
Development Administration under Contract W-7405-ENG-48

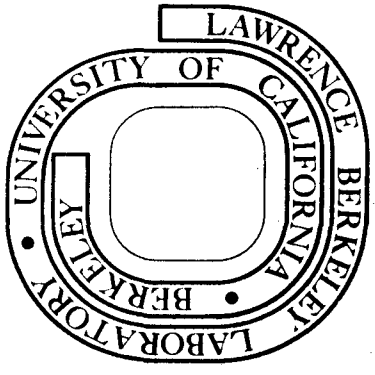

DISCLAIMER

FILAMENTARY NIOBIUM-TIN SUPERCONDUCTORS FABRICATED BY A POWDER METALLURGY APPROACH

Contents

FILAMENTARY NIOBIUM-TIN SUPERCONDUCTORS FABRICATED BY A POWDER METALLURGY APPROACH

Kanithi Hemachalam

Materials and Molecular Research Division, Lawrence Berkeley Laboratory
and Department of Mechanical Engineering, University of California
Berkeley, California 94720

ABSTRACT

Procedures are described for making superconducting tapes and wires containing filaments of the A-15 compound, Nb_3Sn, by powder metallurgy techniques. The fabrication involves achieving a controlled porosity in compacts of sintered niobium followed by tin infiltration and mechanical reduction. The Nb_3Sn filaments, typically 1-5 μm thick, are formed by a short heat treatment.

The effects of certain process variables on the microstructure of the tapes and wires were investigated. Microstructural aspects were examined by optical metallography and transmission electron microscopy. A pulsed field technique was used to determine the critical current density, J_c, at 4.2°K as a function of transverse magnetic field up to 170 kG. Satisfactory agreement was observed between these results and data obtained under steady fields of up to 100 kG. The J_c of the conductors are related to their individual filament morphologies resulting from the different thermo-mechanical histories. The effect of heat treatment conditions on critical current and transition temperature, T_c, is presented. Through process modifications, optimal values or ranges are developed for the metallurgical variables in order to maximize the superconducting properties.

The inductively measured T_c of the conductors is about 17.9±0.1°. The values of J_c for the wires computed on the basis of Nb_3Sn and niobium matrix are 2.3×10^5 A/cm^2 at a transverse pulse field of 50 kG, 1.1×10^5 A/cm^2 at 100 kG and 7.5×10^4 A/cm^2 at 150 kG. Overall critical current densities of the present wires are compared with that of a commercially available multifilamentary wire. The stability and the magnetization behavior of the wires are evaluated under time-varying fields of up to 28 kG/sec. Mechanical tests were conducted to assess the degradation of current-carrying capacity with bending diameter. These results indicate that the conductors produced by the new powder approach have a great potential for superconducting magnets.

I. INTRODUCTION

Applications of superconducting materials to energy conversion, storage and transmission systems, high energy particle accelerators as well as mass transit trains are being seriously investigated at the present time. The realization of the full potential of superconducting material in these applications appears, however, to depend on the successful development of conductors using A-15 compounds such as Nb_3Sn, Nb_3Al, V_3Ga and Nb_3Ge which have superior critical superconducting properties. The first compound discovered to have high magnetic field properties and magnet potential,[1,2] Nb_3Sn, has undergone considerable study and development during the past 15 years. Because the A_3B type compounds are inherently brittle, special methodologies are required to fabricate them into usable forms. A brief historic review of the major process developments is given in the next section.

At the Materials and Molecular Research Division of the Lawrence Berkeley Laboratory, a unique powder metallurgy approach has been developed to fabricate a flexible filamentary tape.[3,4] The method involves roll compacting powder of component A (for A_3B compound) into a porous strip followed by sintering and infiltration with component B. The strip is them mechanically reduced and heat treated to form the A_3B filaments embedded in the A matrix. Previous investigators Babu[5] and Tom[6] have successfully demonstrated the applicability of this approach to Nb_3Sn and Nb_3Al respectively. This procedure also has the potential for systems such as V-Ga and Nb-Ga in which the second component melts below the diffusion heat treatment temperature.

One objective of the current investigation is to make improvements in the overall current-carrying capacity of the Nb_3Sn filamentary tape, through a variation in the process parameters. One difficulty encountered by Babu[5] was that the impregnated tin escaped during mechanical reduction causing lower volume fractions of Nb_3Sn. In Chapter III, two methods for preventing loss of tin are described. One is hardening the tin with particles of a second phase and the other, cold working the tape at a low temperature.[7] Also described are attempts to enhance the critical current density J_c by doping the tape with zirconium.

By following the basic idea of the powder metallurgy approach, process modifications have been made to fabricate a superconductor in the form of a wire.[8] Chapters IV and V deal with the developmental work for a single core wire and a multicore composite wire respectively. The relative merits of different cladding materials and types of cold reduction are discussed. By reducing the filament size, significant improvements were made in the J_c of the wires as compared to the tapes. A systematic study was conducted to determine the influence of time and temperature of heat treatment on the transition temperature (T_c) and J_c. The dependence of J_c on filament size was also determined. Transmission electron microscopy was employed to study the microstructure of Nb_3Sn with respect to grain size and precipitates. Transition temperatures were measured inductively. Critical current density measurements were made on short samples under transverse fields of up to ~170 kG using a pulse magnet. Some results were compared with data obtained under steady fields of up to 100 kG. The susceptibility

to mechanical damage of the Nb_3Sn filaments was estimated for some wires by measuring the degradation of critical current due to bending. Small 2.5 cm dia coils were wound from representative single core wires, and their magnetization behavior was determined. Hysteresis losses as a function of time rate of change of external field were established. Finally, an attempt is made to understand the magnetization characteristics of the wires on the basis of their filament morphology.

II. HISTORICAL REVIEW

Since 1954 when Matthias[1] discovered the high critical temperature of Nb_3Sn, and especially since 1961 when Kunzler et al.[2] first reported the high magnetic field properties of Nb_3Sn, a new era began in the study and development of superconductors. Because Nb_3Sn is a brittle compound, conductor fabrication required special techniques. The first usable A-15 superconductor was made by a powder core wire process[2,9,10] in which a mixture of niobium and tin powders was packed inside a niobium tube and reduced to a fine wire. The superconductive Nb_3Sn core had to be formed via a high temperature (900°C) heat treatment after the conductor was would into its final magnet configuration. The disadvantages of this "wind and react" procedure, namely, the difficulty of getting a uniform core from a powder mixture on a production basis, of finding an insulation to withstand the heat treatment, and the occurrence of "magnetic instabilities" have made the process virtually obsolete.

Another pioneering approach was that by Hanak et al.[11,12] who combined the high current density of an Nb_3Sn layer obtained through a chemical vapor-phase deposition with the necessary mechanical strength contributed by a Hastalloy wire or ribbon substrate. In this RCA process a mixture of niobium and tin clorides was reduced with hydrogen resulting in a deposit of Nb_3Sn on the hot substrate. The early high field devices designed and built utilizing this ribbon conductor had demonstrated the basic technical soundness of this approach. However, the economics of the process and the market situation apparently forced its original developers to reassess

their commitment to this type of product.

In a third major approach developed by the General Electric Company and now called the "G. E. process", tin is coated on a niobium tape and a thin layer of Nb_3Sn is formed on either side of the type by a diffusion treatment.[13,14] Two layers of high conductivity copper or aluminum for cryogenic stability and a layer of stainless steel for mechanical strength are added on the diffused ribbon to make it a flexible, practical conductor. The G. E. diffusion process has also been adapted to form multistrand wire by drawing down a number of tin-coated niobium wires together in a nobium or copper jacket, and then heat treating the assembly.[15,16]

The development of multifilamentary wire by Tachikawa[17,18] in 1967 resulted in a process that has been extensively explored in the recent past to fabricate an intrinsically stable filamentary conductor.[19-23] The desired multifilament configuration is processed by drawing a composite of niobium wires in a copper-tin alloy matrix. Cut sections of this drawn composite are bundled in tubing and redrawn. The procedure is repeated until the desired niobium filament size is obtained. Nb_3Sn is then formed at the interface of niobium and the matrix by a lengthy (10-200 hr) solid-state diffusion reaction at 600-700°C. The bronze matrix can be replaced by pure copper to eliminate the need for annealing of the bronze during mechanical reduction. The necessary tin is later applied externally and is diffused through. The solid-state diffusion approach which can be adapted to other superconductor systems as well (for e.g., V-Ga and V-Si[23]) is currently employed on a commercial basis to produce Nb_3Sn and V_3Ga multifilamentary composite wires.[24-26]

Among other major process developments of the 1970's are the twisted filamentary ribbon by Coles[27,28] and the casting technique by Tsuei.[29-31] The filamentary ribbon process is based on photoresist etching, utilized in printed circuit technology, to establish discrete helical current paths; the Nb_3Sn itself is produced by the G. E. diffusion method. While the improved stability is an advantage, the current densities attained so far are low compared to the conventional ribbon. The production of long lengths also seems to be prohibitively expensive. In Tsuei's casting technique, a copper alloy casting containing small amounts of tin and niobium precipitates is heavily cold-worked to elongate the niobium into thin filaments. After a long solid-state diffusion heat treatment the niobium filaments are partially converted into Nb_3Sn. The overlapping interfilament distance being very small, the currents are carried by a proximity effect. Because of its simplicity, this approach has a potential for large scale production to filamentary conductors. The realization of only small overall current densities thus far, perhaps puts a restriction on the use of these conductors to applications like power transmission where low magnetic fields are involved.

III. PROCESSING OF TAPES AND RELATED STUDIES

The normal procedure for making the niobium-tin tape by the powder metallurgy techniques is as follows. Niobium powder of 99.9% purity having a maximum particle size of 44 microns and a particle size distribution as shown in Table I, was rolled into a self supporting porous strip. The strip was then sintered in a vacuum of $1\text{-}3\times10^{-4}$ mm Hg at a temperature between 2200-2300°C for 3 to 5 min. The result was a ductile tape with a definite volume fraction of interconnected pores. The pores were filled with tin by immersing the sintered tape for 1 min in a 650°C tin bath contained in a graphite crucible. Flat-rolling the infiltrated tape at room temperature to a reduction in thickness of 75 to 90% established the desired morphology. The deformation caused a pronounced elongation of the tin and resulted in a composite consisting of thin filaments of tin arrayed in a niobium matrix. A thermal treatment for approximately 3 to 5 min at 950-100°C converted the material into a superconducting composite in which thin filaments of Nb_3Sn phase were dispersed in a niobium matrix.

Because of the difference in flow stress between niobium and tin, some of the latter was squeezed out to the surface at severe reductions in thickness. The loss of tin significantly reduced the volume fraction of Nb_3Sn and resulted in a lower current-carrying capacity than would have been anticipated from the amount of tin in the infiltrated tape. Several methods were devised for retaining as much of the tin as possible. In one, the infiltrated tape was rolled at a temperature of -72°C. It was expected that the increase flow

stress of tin at the low temperature would reduce the squeeze-out. This was indeed the result.

In a second modification, 2% by weight of copper was added to the molten tin bath. The limited solid solubility of copper in tin resulted in a dispersion of Cu_6Sn_5 crystallites that hardened the tin. However, it was observed after the rolling operation that these crystallites were too large to be accommodated in the tin filaments of tin. Therefore, in an alternate attempt, tin was hardened by a controlled inclusion of intermediate phases. Reference to Fig. 1, a phase diagram for the niobium-tin system, shows that after the usual impregnation at 650°C, it is thermodynamically possible to have Nb, Nb_3Sn, Nb_6Sn_5, $NbSn_2$ and Sn all present in the same infiltrated tape. However, the reaction kinetics at this temperature for the short immersion times employed are such that virtually none of the intermediate phases is present, as may be seen in Fig. 2(a). If the infiltration temperature is increased to 850°C, there is a marked change in the reaction kinetics. Figure 2(b) shows a tape infiltrated at 850°C for 30 sec. It contains a considerable amount of intermediate phases, predominantly Nb_6Sn_5 which is readily distinguished by the characteristic reddish brown color imparted by anodic etching. A tape that had been infiltrated at 850°, rolled at room temperature and heat treated at 970°C for 5 min is illustrated in Fig. 3(c). Figures 3(a) and 3(b) show typical longitudinal sections of tapes produced by "normal" processing and cryogenic rolling respectively. The progressive increase in the volume fraction of the dark Nb_3Sn filaments from Fig. 3(a) to Fig. 3(c) is readily apparent.

It is well known that imperfections such as dislocations, grain boundaries and second phase inclusions in a superconducting material increase the intrinsic critical current density J_c. The defects effectively pin fluxons which in the absence of defects move due to Lorentz force, (I×H), causing a voltage. In practive, superconductors are doped with materials such as zirconium.[32,33] After being precipitated as oxide particles, these dopants lead to a fine grain size and retard further grain growth.

In the present tape-making procedure, 1.5 at.% Zr was added to the infiltrant tin contained in a quartz crucible. A graphite crucible could not be used due to formation of ZrC which hindered wetting of sintered Nb strip by the molten tin alloy. Alternatively, a Nb-1.5 at.% Zr powder was prepared by a hydride technique and was employed in place of pure Nb powder.

IV. PROCESSING OF SINGLE CORE WIRES

A. Philosophy Behind Wire Making

When a superconductor is operating in the mixed state i.e., H_{c1}< applied field <H_{c2}, any perturbation (for example, a change in applied magnetic field) can cause movement of flux lines resulting in a voltage. If the voltage is large enough, the heat generated will locally drive the superconductor normal. Consequently, this puts more current load on the remaining portion driving it normal if its J_c is exceeded. This process is commonly known as a "quench", or an "instability" of a superconductor. To circumvent the problem of instability, several criteria[34,35] have been derived to serve as guide lines in the design of intrinsically stable practical superconductors. Smith, et al. have developed an adiabatic stability criterion that assumes no heat loss from the superconductor during the perturbation. The criterion limits the superconductor filament size x by the following relation.

$$x < \left(10^9 \pi C_p T_o\right)^{0.5}/4J_c$$

where

$$T_o = J_c/(-dJ_c/dT)$$

C_p is the specific heat and J_c the critical current density of the superconducting material. This relationship yields a value of Nb_3Sn filament size of the order of 10 μm or less for stable performance. Further, Hancox[36,37] has shown that with sufficiently fine filaments, partial flux jumps may not quench the transport current.

In the P/M tape-process, the width of the tape is not altered due to the plane strain mechanical reduction. Thus, as can be seen in Fig. 4, the final filament width is typically 40-60 μm, approximately the size of an infiltrated pore. Even though the filament thickness is only about 3-6 μm, the most critical dimension is filament width if the applied field is perpendicular to the plane of the tape. Therefore, the reduction by a factor of 4 to 6 in the filament width is necessary to make the conductor intrinsically stable. Consequently, modifications were made to adapt the main features of the tape-process for fabricating the superconductor in the form of a wire. A wire form provides an additional advantage besides stability. Suitably clad, the single wire can be used as a basic element of a flexible multicore conductor or a transposed multistrand cable to carry large currents. Figure 5 illustrates the essential steps in the wire making process.

B. Process Development

1. Sintering and Infiltration

Two variations of sintering were employed to produce cylindrical niobium rods with the required volume fraction of interconnected pores. In one, several batches of niobium powder with different particle-size ranges were separately pressureless sintered in mullite tubes for ~5 min at 1600°C. Self supporting rods 4.0 mm in dia were obtained when the mullite tubes were removed. The rods were resintered for 10 to 12 min at 2250 to 2300°C in a vacuum of $5\text{-}8\times10^{-5}$ mm Hg. The porous rods thus obtained were infiltrated with tin by immersing them for ~30 sec in a 700°C tin bath. Both sintering and infiltration were accomplished in an Abar furnace. A schematic diagram, Fig. 6,

illustrates the essential features of the furnace. Cross sections of the infiltrated rods made with different grades of niobium powder are shown in Fig. 7. It can be readily seen that -400 mesh powder (Fig. 7(b)) resulted in a porosity ~20%, comparable to that of powder-rolled tape. The other powder fraction (-325+400 mesh) produced porosity (or tin) levels much beyond the 30% necessary to convert all the niobium into Nb_3Sn.

In the second variation, niobium powder was packed in rubber molds and isostatically compacted at 173-207 N/mm^2 (25-30 ksi) into self supporting rods. These rods were then vacuum sintered for 10-15 min in the 2250-2300°C range. Infiltration with tin was performed in the manner described previously. Figure 8 shows typical cross-sections of infiltrated rods made from (a) -270 mesh and (b) -270+400 mesh powder. The latter appears to result in a more uniform pore size. Because of the relative ease of fabrication, the isostatic compaction was employed for all the wires whose properties will be reported later.

2. Cladding

Cladding the infiltrated rods was necessary to prevent loss of tin and to impart support during mechanical deformation. Therefore, the rods were first ensheathed within a niobium or tantalum tube. Because of the susceptibility of both niobium and tantalum to galling, the assemblies were reclad in tubing of another metal having a much lower galling tendency when the deformation mode to be used was wire drawing. Copper and monel were separately used as the exterior clad. The intermediate sheath (niobium or tantalum) was to serve as a

diffusion barrier preventing any reaction between the outer sheath and the infiltrated core during the high temperature diffusion heat treatment. For some wires, the expensive interior sheath was eliminated to determine the extent of reaction between the monel and the core.

3. Mechanical Reduction

In order to elongate the tin in the porous niobium rods, clad assemblies had to be subjected to a suitable mode of deformation. Therefore, the assemblies were reduced to wire by one or a combination of the following deformation processes: swaging, form rolling and wire drawing. A metallographic study (Fig. 9(a)) of wire sections has indicated that swaging produced a characteristic structure related to the severe twisting action of the rotating hammers. As can be seen from Figs. 9(b) and 9(c), form rolling followed by wire drawing, and wire drawing alone, yielded wires with much more isotropic cross-section than the fully swaged one. Prior to the final wire drawing, form rolling the composites to about 2.5 mm o.d. using the rolling mill shown in Fig. 10 proved especially useful for an increased speed of wire production. By these two deformation methods reduction ratios (initial cross section area of infiltrated rod ÷ final cross sectional area of the core) of up to 500 were realized on some wires. A laboratory built drawing bench (Fig. 11) equipped with an air motor was used for wire drawing. Of the several commercial lubricants tested in wire drawing Vidax AR, a suspension of teflon in trichlorotri-fluoroethane (supplied by DuPont), required the lowest load for a given reduction.[38] Consequently, Vidax AR was used as a

lubricant in all the wire drawing operations.

One serious problem faced in the deformation of the composite was the wrinkling of the niobium or tantalum jacket. This wrinkling, in conjunction with the various defects of commercial niobium tubes, some times led to wire breakage. This problem was partly solved by using annealed tubes of niobium or tantalum made from a rod. Furthermore, since the grooves in the rolling mill were rectangular, use of a copper tube with a round hole and a square outer section as an exterior cladding resulted in a cylindrical core and less wrinkling of the tantalum sheath.

4. Diffusion Treatment

The diffusion heat treatment was carried out on wire samples at temperatures ranging from 750°C to 1200°C and for times varying from 1 min to 2 hr. Before heat treatment, samples were either encapsulated in argon filled quartz tubes or sealed in stainless steel bags purged with argon. While both the methods proved satisfactory, the latter was especially convenient for heat treating long sections of the wire. After the exposure at temperature, the samples along with their containers were normally cooled in water.

For temperatures and durations tried, the heat treatment resulted in no observable reaction between the diffusion barrier niobium (or tantalum) and the exterior sheath. However, in wires without the diffusion barrier, three brittle reaction layers of varying thickness were formed between the central core and the monel cladding. Figures 12(b) and 12(c) show these layers for two wires that had been thermally treated for 3 min at 900°C and 1 min at 930°C respectively. Figure 12(a)

is a cross-section of an unreacted specimen. The influence of this reaction on T_c and J_c will be reported in Chapter VII under results and discussion. For wires with only copper as the cladding, a rapid mixing of copper and tin occurred upon heating. The resulting bronze greatly retarded the formation of Nb_3Sn.

V. PROCESSING OF MULTICORE WIRES

A preliminary investigation on multicore wires was conducted for the following reasons: to find out if the sintered and infiltrated core would lend itself to the high reduction ratios beyond 500 necessary for multicore composites; and to determine possible J_c improvements due to submicron filament size. Two series of wires containing 6 and 7 cores were prepared by a bundling and co-reducing process. In one set, the monel jacket of the single core wire was dissolved in a 50% nitric acid solution leaving the tantalum sheath protecting the core. The wire then measured 1.2 mm o.d. Six 10 cm long sections of the wire were placed around a 1.2 mm dia copper wire and the bundle was inserted in an annealed monel tube. The purpose of the central copper core was to provide a thermal and electrical shunt when operating in the mixed state. The multicore assembly was then wire drawn to ~0.66 mm 0.d. when the cores began to break internally. Sections of the wire without breaks were saved and heat treated for 1 to 2 min at 950°C in a manner previously described. Figure 13(a) shows the cross-section of a diffusion treated 6-core wire. It is important to note that the copper core, being totally surrounded by the tantalum clad superconductor cores, was not contaminated by the outside monel during the heat treatment.

The second series of multicore conductors were made from monel-clad single core wire that did not have the tantalum barrier. Seven sections of 0.66 mm o.d. wire were assembled in a monel tube. The composite was then form rolled and wire drawn to ~0.75 mm o.d. when core breakage was noticed. Figure 13(b) shows a cross-section of the

multicore wire reacted for 1 min at 930°C. The characteristic reaction layers between the cores and the monel jacket were observed under a high magnification.

VI. CHARACTERIZATION TECHNIQUES

A. Metallography

1. Optical Metallography

An anodic oxidation method developed by Picklesimer[39] proved indenspensable in identifying niobium, tin and their intermetallic compounds present in samples. The anodization resulted in characteristic colors for each phase: light blue for Nb, dark blue or violet for Nb_3Sn, reddish brown for Nb_6Sn_5 and yellow for Sn. Anodized tantalum had a violet color much deeper than Nb_3Sn. However, in the presence of either copper or monel claddings, the anodization produced phase colors that were indistinguishable. Therefore, the clads were normally dissolved in nitric acid before the specimens were set in Koldmount. Chemical etching of polished samples in a solution containing equal parts of HNO_3 and CH_3COOH was employed for observing reaction layers between monel and the infiltrated core. Volume fractions of tin and Nb_3Sn were estimated, when necessary, by cutting and weighing the individual phases from micrographs.

2. Electron Microscopy

Transmission electron microscopy, TEM, was employed to investigate Nb_3Sn grain size and the presence of second phase particles. Samples were prepared by a technique similar to the one described by Scanlan et al.[40] A single-core composite with tantalum and monel claddings was form rolled to 2.5 mm o.d., drawn to 1.7 mm o.d. and then flat rolled into a ribbon about 0.1 mm thick and 3 mm wide. The flat rolling operation produced a cross-section more suitable than round wires for subsequent thinning for TEM. The outer monel clad was

removed from the tape by dissolving it in nitric acid. Small lengths of this tape were heat treated in argon for various times at 950°-1100°C. 2.3 mm discs were spark-cut from the tape and the exterior tantalum sheaths were carefully removed to obtain central plates approximately 0.04 mm thick. These discs were than placed in a Technics ion micromilling instrument in which argon beams directed onto both sides of the specimen slowly sputter away material until holes appear through the sample. Micromilled discs were stored in a vacuum dessicator (to prevent any oxidation of the thinned areas) prior to their examination in a Siemens IA electron microscope at an operating voltage of 100 kV. Since the Nb_3Sn filaments were only several microns wide, it was possible to photograph grains of both Nb_3Sn and Nb simultaneously at a magnification of about 23,000. The Nb_3Sn phase could easily be identified by the clarity of its grains as well as its selected area diffraction pattern. Niobium, on the other hand, showed a marked cold worked structure and a body centered cubic diffraction pattern.

B. Transition Temperature Measurements

The superconducting-to-normal transition temperature T_c of samples was determined inductively. In principle, the inductive method relies on the fact that the self-inductance and the frequency of a coil around the sample vary with the magnetic permeability of the samples. The method has the advantage that it requires no direct electrical contacts with the sample, and that it may be used for samples of irregular shapes.

The experimental setup is shown in the block diagram in Fig. 14. The setup provided an isothermal space containing a Manganin wire

heater and an Au-7 at.% Fe thermocouple. Cooling was achieved by the evaporation of helium through the bottom end of the probe at a constant rate. The amplified output of the thermocouple drives both the x-axis of a chart recorder and a feedback system of the heater controller. The susceptibility of the sample was measured by a standard Schawlow-Devlin resonance method[41] with an added detector circuit that extracts the frequency shift and power loss in the resonant coil circuit. The coil had a resonant frequency of 41 kHz and a peak field of ~75 mG. The transition temperature was measured by recording the frequency shift as the sample changed from the superconducting to the normal state during heating. The temperatures measured by the apparatus were believed to be accurate within 0.1°K.

C. Critical Current Measurements

Two methods were employed to measure the magnetic field dependence of critical current density for tapes and wires processed by the P/M techniques. In one, samples were tested in a superconducting dc magnet capable of developing steady magnetic fields of up to 100 kG. The second method consisted of utilizing a pulse magnet that could generate transient fields beyond 100 kG. Both the tests were conducted at 4.2°K. Because of the relative ease of operation, the latter testing procedure was used to evaluate most specimens.

1. Steady Field Technique

The steady field magnet consisted of two concentric solenoids connected in series, each capable of generating ~50 kG. The outer solenoid was made from a single-filament Nb-Ti wire and the inner from a Nb_3Sn tape. The magnet bore had an effective diameter of 5 cm and

a length of 38 cm. Thermally treated wire sections, each 70 cm long, were tightly would on a 3.8 cm dia holder, as shown in Fig. 15(a). Since the winding entailed a rather sharp bend at the middle of the wire, the central portion had been preformed before the heat treatment. Soldered current leads overlapped about 5 cm of the sample wire. Voltage connections were made in order to measure the potential across a 50 cm length of wire.

The testing procedure consisted of cooling the sample probe with liquid nitrogen before placing it in the superconducting magnet immersed in liquid helium. The arrangement of sample coil in the magnet bore was such that the field was transverse to the transport current. After the magnet was charged to a desired field strength, the current in the sample was gradually increased until a transition to the normal state occurred. The transport current and the voltage drop in the sample were simultaneously recorded in a Clevite-Brush 6-channel recorder with a maximum sensitivity of 1 μV. Transitions from the superconducting to normal state were recorded at least three times in order to observe any "training" the wire might show. However, the variations in the critical currents were almost negligible for each specimen. The above procedure was repeated at different field settings to obtain a J_c vs H plot over the feasible range of 0-100 kG.

2. Pulsed Field Technique

Superconductor samples were tested at 4.2°K for current-carrying behavior using a pulse magnet (Fig. 16(a)) capable of producing field strengths H in excess of 200 kG. The time for the pulse to rise from zero field to peak was approximately 8 milliseconds. The orientation

of transport current in the sample with respect to the field, as well as the main features of the pulse magnet apparatus, are shown schematically in Fig. 16(b). For determining the J_c vs H relationship, a method described in Chabanne[42] and Garrett[43] was employed. In order to have the pulse-field data correlate well with steady field results, dH/dt should be as nearly zero as possible. This condition was achieved by controlling the magnet field so that for a set sample current, the resistive transition occurred very close to the peak of the field pulse. A typical oscilloscope record of the sample current, the magnetic field and the voltage drop across the sample is illustrated in Fig. 17. To prevent overheating of the test specimens after the upper transition had occurred, the sample current was automatically cut off just beyond the peak of the field pulse.

The word of caution is necessary in regard to the sample mounting. When a short straight sample is soldered between the current leads, the transport current can create hot-spots at the solder joints. These hot-spots can easily raise the sample temperature near the potential contacts leading to erroneous J_c measurements. To circumvent this difficulty, a previously bent and reacted wire sample was mounted. As can be seen in Fig. 15(b), the current transfer length as well as the separation of the current joints from the voltage connections were increased. In the case of testing superconducting tapes, U-shaped sections were carefully cut before mounting on the probe.

D. Magnetization Measurements

A standard "bucking" technique was used to obtain the magnetization behavior of several single core wires. The block diagram in Fig. 18 indicates the salient features of the apparatus. Wires, each approximately 250 cm long, were individually wound on 2.54 cm dia bobbins with a nylon string separating the turns, as shown in Fig. 15(c). The sample was placed in one of a pair of search coils situated in a time-dependent magnetic field. These coils were connected in series-opposition so that there was no signal in the absence of a sample. Thus, with the sample in place, the integrated output voltage from the bucking coils was proportional to the sample magnetization.[34] The external field was generated by a superconducting magnet wound with a Nb-Ti multistrand-multifilamentary wire. This 10 cm high and 5 cm bore magnet was capable of producing a maximum peak field of ~46 kG. The maximum and minimum field rates attainable were ~28 kG/sec and ~1.1 kG/sec respectively. The former value was limited by the power supply voltage; the latter by internal drift of the integrator.

The output from the integrator was fed to the Y-axis of an XY plotter. The X-axis input was from a magnet-current measuring shunt whose signal was proportional to the field strength B. With the peak field set at a constant value, several magnetization curves were recorded for different magnitudes of B. The areas of each loop, a measure of hysteresis losses in the sample, were simultaneously determined by a Digital-Multiplier-Integrator circuit[44] (not shown in Fig. 18). The above procedure was repeated for a few other values of peak field.

E. Mechanical Properties

The susceptibility of a superconductor to mechanical damage can limit its usefulness for some applications. Since wires are subjected to severe treatment in operations such as coil winding, cabling and braiding, their current-carrying capacity can be easily degraded. The decrease in critical current due to bending of a single core wire was evaluated by wrapping 15 cm long wires around a mandrel, straightening them and measuring the critical current. The same samples were bent around successively smaller mandrels. The tests were conducted at 4.2°K under a steady magnetic field of 50 kG perpendicular to the transport current. Distance between potential leads was 2.5 cm. The bend-test data are discussed in Chapter VII.

VII. RESULTS AND DISCUSSION

A. Transition Temperature

The superconducting transition temperature, T_c, was inductively measured for samples heat treated in the temperature range 750-1200°C. The critical temperature was defined as the temperature corresponding to the midpoint of the frequency change at transition. The T_c of wires with tantalum-clad 3 mm dia cores is shown in Fig. 19 as a function of Nb_3Sn formation temperature. The width of the transition ΔT, indicated by vertical bars, was defined as the temperature difference between 10% and 100% of the total inductance signal. The 10% limit was arbitrarily chosen because of a gradual change in the output signal at the beginning of the transition from superconducting to normal state. As shown in Fig. 20, the end of transition (also referred to as the "onset" while cooling) was much sharper than the beginning.

The wires heat treated in the range 900-1200°C had an exposure time of only 2 min at temperature. The three specimens reacted for 1 hr at 750°, 800° and 950°C respectively, had the same values of T_c and ΔT as the ones heat treated for 2 min at each temperature. However, the longer reaction at 750° and 800°C resulted in an inductance signal greater than the corresponding 2 min durations. This is to be expected because of the sluggish formation of Nb_3Sn and fast growth of other intermetallic compounds at these low temperatures. The absence of any noticeable change in the signal for the 950°C specimens heat treated for 2 min and 1 hr respectively, suggests that the reaction was complete in only 2 min.

In spite of the short heat treatment, the T_c values plotted in Fig. 19 are in general agreement with those reported in the literature[2,45,46] for sintered Nb_3Sn. The slightly higher values, 18.2-18.3, measured by other researchers[5,47] are considered to be the result of a resistive method employed for T_c determination. Since the current through the specimen is very small, the resistive transition may sample a continuous but extremely small, high-T_c region of the specimen. On the other hand, the resonant coil in the inductive method senses the bulk of the superconducting material, thereby indicating the variation of T_c within the compound. This was in fact observed as shown in Fig. 20, for a superconducting tape processed from a 1.5% zirconium doped niobium powder. The T_c of the doped material was 17.2°K and the ΔT was 1.3°K. Such broad transitions and lower critical temperatures as compared to those of undoped material (Fig. 20) have been reported by others (e.g., Suenaga et al. in Ref. 33) for multifilamentary Nb_3Sn wires doped with zirconium. A possible reason for the low T_c and broad ΔT is the existence of regions containing small grains of Nb_3Sn and precipitates of ZrO_2. These precipitates and the increased density of grain boundaries may disturb the long-range crystallographic order[48,49] necessary for high T_c in A-15 compounds. It has been established[49,50] that the integrity of A atom chains in the A_3B structure must be maintained for the maximum attainable T_c. The observed reductions in the T_c of specimens reacted below 900°C (Fig. 19) may be explained on the basis of a lack of enough atomic mobility to achieve the crystallographic order in the reaction times employed.

For monel-clad wires that did not have any diffusion barrier the T_c and ΔT were 17.9°K and 0.35°K respectively. These values indicate that the brittle reaction layers formed between the monel and the core during a 1 min heat treatment at 930°C did not degrade the critical temperature of the superconducting material.

B. Pulsed Fields vs Steady Fields

Pulsed field techniques[51-54] have long been employed for investigating critical fields of various superconductors. However, comparisons of pulsed-field behavior with observations in steady fields so far have been scanty. Often the critical current vs magnetic field characteristics reported in the two kinds of fields have differed substantially because of variations in experimental techniques and in definitions of the superconducting properties. In the present study, current densities of several P/M processed wires were measured using both pulsed and steady field techniques as described in Chapter VI. Typical results are plotted in Fig. 21. Pulsed field values corresponding to the end of the resistive transition shown in Fig. 17 were used for computing the J_c vs H characteristics. In the case of tests performed under steady fields, the current densities were determined at a resistivity of 10^{-12} Ω-cm. As can be seen from Fig. 21, there is good agreement between the two sets of data at high fields. However, at fields below 50 kG, the critical current densities measured under pulsed fields are low relative to the values determined in steady fields. This disagreement is attributed to joule heating at the current contacts of the short sample used in the pulsed field tests. The critical currents at these low fields range between 100A

and 200A. The transfer of such large currents may create enough heat at the solder joints to raise the specimen temperature thus influencing the results.

Babu[5] has studied the current-carrying behavior of powder-rolled tape under pulsed and steady fields. According to his results, the two sets of data match when the steady field J_c is calculated at a resistivity of $\sim 5\times10^{-9}$ Ω-cm. A possible reason for the apparent discrepancy in the matching resistivity levels of tapes and wires is the fact that the resistive transition in pulsed fields is much broader for the tapes than for the wires. The transition width for wires was always less than 5% of the peak field while the transition extended up to about 30% for tape samples. Indications are that if the start of the resistive transition had been taken as the criterion for determining the critical field for the tapes, the current-carrying behavior in pulsed fields would have matched with the steady field data at a resistivity level close to 10^{-12} Ω-cm.

C. Critical Current Density of Tapes

Critical current density values J_c were determined on the basis of the entire cross-section of the tape, exclusive of the surface coating of tin. Reporting the data in this manner circumvents the uncertainties involved in the determination of the Nb_3Sn volume fraction which is required for calculating the intrinsic critical current density of the superconducting phase. These uncertainties

arise from the complex filament morphology, a characteristic of the present P/M approach. Furthermore, since the overall current density depends on both the intrinsic critical current density and the volume fraction of Nb_3Sn, the J_c computed as above provides a meaningful indication of the merit of the tape as a practical superconductor.

Brief processing histories of tapes that were tested under pulsed fields are presented in Table II. The dependence of J_c on the transverse magnetic field of three tapes with different thermo-mechanical histories is shown in Fig. 22. As can be seen, the cryogenically rolled tape 2, carried higher currents than the normally processed tape 1. However, tape 3 which had a high temperature tin infiltration, performed better than both 1 and 2. The purpose of the high temperature infiltration was to harden the tin by the formation of tin-rich intermetallic phases. Approximate Nb_3Sn volume fraction determined from their cross-sectional photomicrographs (Fig. 3) were 30% for tape 1, 40% for tape 2 and 50% for tape 3. As was anticipated, the ratios of J_c for a given field taken from the three curves of Fig. 22 are found to agree well with the corresponding ratios of the volume fractions. These findings clearly indicate that the high temperature infiltration is effective in preventing loss of tin during mechanical reduction.

The influence of zirconium doping on the current-carrying behavior of the tapes is shown in Fig. 23. The dopant was introduced either through the infiltrant tin (tape 4) or in the niobium powder (tape 5). Tape 1 was undoped. Since the volume fraction of Nb_3Sn in both of the doped tapes is nearly equal, it is obvious from Fig. 22 that the

doping is most effective in raising the critical current density of Nb_3Sn only when the zirconium is added to the starting niobium powder.

D. Critical Current Density of Wires

1. Effect of Deformation Mode

In order to find the best mode of deformation, wire samples fabricated by different mechanical reduction processes were tested for current-carrying capacity under pulsed magnetic fields. Because of the limited ductility of initial batches of sintered rods, all the infiltrated cores were reduced to a diameter of 0.45 mm. The critical current density based on the entire core is shown in Fig. 24 as a function of transverse field. The three curves were obtained from wires whose cross sections are shown in Figs. 9(a), 9(b) and 9(c). The wires that had been reduced by wire drawing, and by form rolling followed by wire drawing carried more than twice the amount of current carried by the fully swaged one. Partial form rolling prior to swaging improved the J_c vs H characteristics of the wire only slightly (not plotted in Fig. 24) over the fully swaged wire. Since the volume fraction of Nb_3Sn appears to be the same for all the wires, the marked difference in their critical current densities must be related to the nature of the filament disposition in the conductor itself.

2. Effect of Heat Treatment

Single-core wires reacted at temperatures in the range 700-1200°C for times varying from 1 min to several hours were tested in an attempt to optimize the current-carrying behavior of undoped Nb_3Sn wires. The specimens selected for this study were made from isostatically compacted -325+400 mesh niobium powder. Tantalum and monel were

employed as claddings. The diameter of the cores was 0.3 mm after reduction by form rolling and wire drawing. Longitudinal and cross sectional micrographs of reacted wires as typified by those in Figs. 25(a) and 25(b) respectively, indicate the Nb_3Sn filament size to be approximately 1-2 μm. Figure 26 shows a plot of the results of tests on 4 specimens reacted at 800°C for 2, 8, 30 and 120 min respectively. There is a substantial improvement in the overall critical current density of the central core as the reaction time is increased. These results are in general agreement with metallographic observations which showed a progressive growth of the Nb_3Sn layer with time. A metallographic examination of the specimen heat treated for 2 hr at 800°C indicated a complete reaction of the tin. Thus, significant improvements in the critical current behavior of the wires by heat treatments longer than 2 hr at 800°C appear unlikely.

For all the above specimens, the overall critical current density of the core is surprisingly high in view of the reported fact that predominantly $NbSn_2$ and traces of Nb_6Sn_5 form below 845±7°C, the peritectic temperature of $NbSn_2$.[55] As can be seen from the niobium-tin equilibrium phase diagram in Fig. 1, none of the tin-rich intermetallics is stable above 930±8°C. The rate of growth of Nb_3Sn is high at 950°C;[55] consequently, the formation of Nb_3Sn is virtually complete in as short a time as 2 min. This can be easily seen from Fig. 27 in which current data are plotted from seven specimens heat treated for times ranging from 1 to 60 min at 950°C. The 1 min heat treatment resulted in relatively lower current densities at all fields indicating an incomplete reaction. However, all other samples with 2 min or longer heat

treatments have exactly similar J_c vs H characteristics. The slight scatter in the data points (Fig. 27) is within the experimental error limits of the tests under pulsed fields.

It should be noted here that for specimens reacted at 950°C, no reduction in the overall critical current density has been observed by prolonged heat treatment. Reaction periods up to 30 times the minimum required for a complete reaction have apparently had no detrimental influence on the microstructure of the Nb_3Sn phase. This is consistent with the fact that a transmission electron microscope investigation (Figs. 28(a) and 28(b)) of the microstructure has revealed that no noticeable grain growth occurred when the reaction time was increased from 2 min to 30 min. The grains are nearly equiaxed with an average size of ~0.5 μm. Such a fine grain structure formed at the liquid tin-niobium interface was possible in the G.E. diffusion-processed tape only by doping the niobium with zirconium.[32] In the present approach to wire fabrication, the sintered niobium is severely cold worked prior to the final heat treatment. The dense dislocation networks thus introduced in the niobium are believed to serve the purpose of the dopant to some extent in creating nucleation sites for the formation of fine-grained Nb_3Sn.

In Fig. 29, additional results are plotted for the 0.3 mm dia core specimens subjected to a 2 min heat treatment at 950°, 1000°, 1100° and 1200°C respectively. There is a pronounced degradation in the current-carrying capacity as the reaction temperature is increased above 1000°C. Progressively larger grains formed at 1100° and 1200°C are considered to be mainly responsible for such a behavior. In a

sample heat treated for 2 min at 1100°C, transmission electron microscopy has, indeed, revealed a grain size twice that in a specimen reacted for 2 min at 950°C

The variation of overall critical current density with reaction temperature is shown in Fig. 30 for three convenient magnetic field values. The reaction times at 700°C, 800°C and 900°C were respectively 50 hr, 2 hr and 30 min. For temperatures of 950° and higher the heat treatment period was 2 min. As found in a metallographic study, the formation of Nb_3Sn was practically complete in all the specimens. It can be readily seen from the three curves in Fig. 30 that a heat treatment in the range 950-1000°C is the optimum with respect to the critical current behavior of the present undoped wires.

From the results reported so far, an interesting observation can be made concerning the grain size of Nb_3Sn in the filamentary conductors. The grains of Nb_3Sn formed at 700°C are smaller than those formed at 950°C.[40] Also, the peritectic temperature of Nb_3Sn being 2130°C, grain growth may be assumed to be insignificant after a 50 hr heat treatment at 700°C. This assumption is not incorrect in view of the results reported by Scanlan et al. in Ref. 40. Thus, the specimen reacted at 700°C should have a higher overall critical current density than a wire which is subjected to a heat treatment at 950°C. However, a comparison of the current-carrying behavior of the specimens has shown no such improvement. This appears to be due to the difference in critical temperature, T_c, in these wires. It is well known[40,56,57] that the T_c directly influences the thermodynamic critical field $H_c(T)$, which is proportional to $T_c\left|1 - (T/T_c)^2\right|$, and which in turn limits the

ultimate critical currents. The 700°C heat treatment resulted in a lower T_c of 16.6°K relative to 17.9°K of the specimens reacted at 950°C. This lower T_c may offset the increase in J_c caused by the finer grain size. The same agrument holds true for the specimen heat treated at 800°C.

3. Effect of Filament Size

Infiltrated rods identical to those employed in the study of diffusion heat treatment were used to investigate the critical current dependence on the filament size of Nb_3Sn. Filaments of different thickness were achieved simply by varying the amount of mechanical reduction in each wire. To ensure complete reaction, the wires were heat treated at 950°C for various times depending on the size of the central core. The overall critical current density of the cores is plotted in Fig. 31 for 6 wires as a function of transverse pulsed-field. These results indicate that the wires with less than about 0.2 mm dia core have reached an optimum current-carrying capacity after a mere 1 min reaction. The strong dependence of the critical current on the amount of reduction is illustrated in Fig. 32. Here, the overall critical current densities at 50, 100 and 150 kG are plotted as a function of the square root of the reduction ratio R (R = cross sectional area of infiltrated rod ÷ cross sectional area of core in the final wire). Since filament size is proportional to the core diameter (and, therefore, inversely proportional to $\sqrt{R}$), values of filament thickness measured from micrographs are also shown on top of Fig. 32. The current density increases less than linearly with the inverse of filament thickness. Since the only major difference

among the wires tested here is the amount of reduction, formation of finer Nb_3Sn grains may be expected in the smaller wires. However, at the very high reductions, it is possible that the increase in the density of dislocation networks in niobium will not be significant enough to reduce the Nb_3Sn grain size noticeably. If this is true, reducing the core diameter beyond a certain value (about 0.2 mm in the present case) will not improve the critical current density.

The heat treatment to form Nb_3Sn always produced submicron pores dispersed in the superconducting phase. This porosity was a result of the density difference between the Nb_3Sn compound and the reacting components. Cross-sectional micrographs shown in Figs. 33(a), 33(b) and 33(d) indicate the distribution of the pores in three wires with 0.4, 0.3 and 0.22 mm dia cores respectively. The pores, 0.2-0.5 μm in size, are dispersed more randomly in the smaller wires, while they tend to cluster in the larger ones. As can be seen by comparing Figs. 33(b) and 33(c), reaction times longer than necessary to convert all the tin into Nb_3Sn did not result in any change in the porosity. It is widely accepted[58,60] that these micro voids along with the grain boundaries effectively pin the flux lines thus improving the J_c vs H characteristics. The microstructural findings seem to be in general agreement with the critical current densities of the various wires reported here. A quantitative understanding of the flux pinning by the voids is difficult in view of the complexities and uncertainties in the pinning mechanism itself.

4. Multicore Wires

Multicore wires fabricated in the manner described in Chapter V were tested in pulsed fields. The J_c of a 6-core wire is shown in Fig. 34 as a function of perpendicular magnetic field. In addition to the six infiltrated cores, the conductor contained a copper core in the center as illustrated in Fig. 13(a). As expected, the J_c which is computed on the basis of the core cross-section is comparable to that of single core wires with similar reduction ratios. However, since the six cores constituted only 17% of the 0.7 mm dia conductor, the overall J_c will be scaled down in direct proportion relative to the values shown in Fig. 34. The presence of a copper core in the present wire reduced the sample voltage signal at the resistive transition forcing the operation of the oscilloscope at its sensitivity limit of ~0.2 mV. The J_c vs H characteristics of the wires containing a bundle of 7 infiltrated cores and no tantalum barrier are not reported here due to the inability of producing sufficient specimen lengths with no breaks in the cores.

In view of the data presented above, it appears that a multiwire cable will probably be a better concept than a multicore conductor. Practical cables to handle a few thousand amperes may be built by braiding several single core wires along with electrical and cryogenic stabilizers, and mechanical strengthening elements. Two obvious advantages of the cables over large solid conductors are: (1) improved stability[34] due to twisting and transposing of the individual wires, and (2) better flexibility due to the freedom of the movement of each wire when the cable is bent.

5. Infiltrated Wires vs Bronze-Processed Wire

Two wires made by the infiltration approach and a commercial bronze-processed wire[61] were tested for current-carrying capacity under pulsed fields. The cross-sectional micrographs of the three wires are shown in Fig. 35. The outside diameter of each wire was 0.32±0.01 mm. The overall critical current density based on the entire cross-section of the wires is plotted in Fig. 36. The infiltrated wires represented by curves 1 and 2 were clad with monel, but only the first wire contained a tantalum diffusion barrier. Both these wires were reacted for 1 min at 930°C. Curve 3 is obtained for the commercial wire containing 1045 filaments of Nb 1 at.% Zr, each 4 μm in diameter. The wire was heat treated for 70 hr at 700°C. The approximate Nb_3Sn filament thickness in all three wires was 2 μm.

As can be seen from Fig. 36, the critical current densities of the undoped infiltrated wires are superior to those of the bronze-processed wire at high magnetic field. Also, the current-carrying capacity of the latter appears to fall more rapidly as the applied field is increased. This behavior is considered to be due to the existence of a major portion of the Nb_3Sn layer having a relatively low T_c.[62] As mentioned earlier, the low T_c limits J_c at high fields. Furthermore, it should be noted that no attempts had been made to optimize the amount of clad material(s) on the infiltrated wires. Consequently, only 25% and 58% of the total cross-sections were composed of the Nb-Nb_3Sn cores in the two wires respectively. For the commercial wire, on the other hand, the central region consisting of the niobium filaments formed about 60% of the entire wire section. Therefore,

there is scope for substantial increases in the overall critical current densities of the infiltrated wires by means of additives and optimization with respect to cladding to core ratio.

Another important observation from the above results is a reduction of approximately 60% in the J_c of the core that had not been ensheathed in tantalum relative to the protected core. The 60% figure is obtained when areas of individual cores are taken into account. As reported earlier, the three brittle layers formed between monel and the core did not alter the T_c of the material. The mechanism responsible for the critical current degradation is not understood at the present time.

E. Magnetization

When a superconductor is subjected to changing magnetic fields, screening currents are created at its surface to oppose the motion of flux through the material. If the field is cycled, the material with the screening currents is driven around its cycle of magnetization. Thus, the magnetization curves of the defect-containing Type II superconductor represent hysteresis losses that occur under ac conditions. These losses are generally dependent on the rate of change of field $\dot{B}$, and they have significant importance in all ac applications of superconductors. In order to investigate the magnetization behavior, several wires made by the present powder metallurgy approach were tested in a manner described earlier.

The two single core wires selected for this study were each 250 cm long and contained infiltrated cores 0.30 and 0.22 mm in diameter respectively. Figure 37(a) shows a typical magnetization

loop obtained for the larger wire when the external field was cycled through 0-17.7-0 kG at a frequency of 2.08 kG/sec. Figures 37(b) and 37(c) are plots obtained at the same $\dot{B}$ but with peak fields (B_{max}) of 35.4 and 46 kG respectively. The downward motion of the magnetization at low fields was due to the ferromagnetic property of the monel cladding. When the monel was removed from the wire by etching, no such initial deflection was recorded. This is indicated in Fig. 37(d). From the area of the magnetization loop shown in Fig. 37(e) for a monel-clad unreacted wire, it is interesting to note that virtually all the energy loss is due to flux trapping in the Nb_3Sn filaments. The little area enclosed by the curve in (e) is probably contributed by the niobium.

The dependence of hysteresis loss on $\dot{B}$ with B_{max} as the parameter is shown in Fig. 38 for the larger wire. Since the testing method has the inherent limitation that the losses can not be evaluated absolutely, the energy dissipation/cycle normalized for a unit volume of the superconducting core is calculated in arbitrary units. The results indicate that the losses in both the wires are essentially independent of $\dot{B}$ up to ~27 kG/sec, the maximum rate studied. This suggests that the measured magnetization is mainly the individual magnetization of the Nb_3Sn filaments themselves and the coupling currents between the filaments are negligible. (The coupling currents are responsible for eddy current losses in the matrix.) This fact is not surprising in view of the numerous interconnections between the filaments--the induced screening currents circulate only within the filaments. In commercial multifilamentary Nb-Ti and Nb_3Sn conductors, the filaments are usually twisted to render them less sensitive to

increases in the frequency. The frequency independent loss behavior of the infiltrated wires is at present encouraging.

As can be seen from Fig. 39, the smaller wire is about three times more lossy than the larger one at all excitations. One reason for the higher losses is the occurrence of flux jumping at fields less than ~5 kG. The recording of a flux jump is shown in the magnetization loop (f) of Fig. 37. It was obtained for the smaller wire from which the monel cladding was removed. The flux jumping was observed in all cases irrespective of excitation rate and peak value of the field. The exact reasons or mechanisms responsible for this magnetic instability phenomenon present only in the coil wound with smaller wire are not yet identified firmly. The variation in the cross section of Nb_3Sn filaments may be contributing to the higher hysteresis losses to some extent. For given excitation conditions, as the filaments get smaller, the volume of the superconducting phase that becomes saturated with critical screening currents increases. Since the losses are proportional to this saturated volume they may be expected to be correspondingly higher for wires with larger mechanical reductions.

Flux jumping was avoided in subsequent testing of the small wire by means of a small bias field of the order of 5 kG. The resulting magnetization loop is shown in Fig. 37(g) for a $\dot{B}$ of 6.5 kG/sec and B_{max} of 46 kG. The losses/cycle normalized for unit volume were found once again to be independent of $\dot{B}$ and were approximately equal to those of the larger wire tested under similar conditions

F. Mechanical Properties

Flexibility is one of the most necessary features of a superconductor. Since all A-15 compounds are inherently brittle, strains as small as 0.2% usually fracture the superconducting phase resulting in a serious degradation of current-carrying capacity. The limiting strains may be caused either by the bending of a conductor in the construction of devices or by magnetic stresses (J×B) on the conductor during operation.

Bend tests on single core wire samples were conducted as described in Section IV-E. The critical current $I_c(D)$ for a bend diameter D, normalized to the initial current prior to bending, $I_c(\infty)$, is shown in Fig. 40. The values of $I_c(D)$ correspond to a core resistivity $\sim 10^{-12}$ Ω-cm. As can be seen from Fig. 40 the wire with 0.16 mm dia core has slightly better bending characteristics than the larger wire with 0.30 mm core. Both these wires contained an intermediate tantalum sheath. The third wire with 0.25 mm dia core did not have any diffusion barrier. Its bending characteristics clearly indicate that the brittle diffusion layers formed between monel and the core did not alter the current carrying behavior as a function of bend diameter. As wrapping diameter was successively reduced, the voltage sustained by the wires at the point of sudden transition to completely normal state gradually increased. This was due to micro cracks developed in the brittle superconducting phase. These micro cracks acting as resistors in the supercurrent paths, lead to current sharing between the filaments and the matrix. Similar current sharing behavior was reported by Suenaga and Sampson[20] for Nb_3Sn multifilamentary wires produced by a

solid state diffusion. A comparison of the present bending test data with those of solid state diffusion wires[20,62,63] indicates that the P/M processed wires are more flexible than the others. While bends of about 2.5 cm dia reduced the current capacity by approximately 20% in the solid state diffusion wires,[20,62] the P/M processed wires suffered an equal decrement at a bending diameter of ~1.5 cm. This improvement in the bending characteristics could be due to two factors: the interconnections of the Nb_3Sn filaments and the variation in the filament size itself. When the larger filaments develop micro cracks as their limiting strain is approached, part of the sample current can be transported via the interconnections to the finer filaments which still may be intact. Such a mechanism is not possible in the solid-state-processed conductor containing parallel filaments that have a uniform thickness throughout

VIII. SUMMARY AND CONCLUSIONS

Based on powder metallurgy techniques, the fabrication of filamentary Nb_3Sn superconductors in the form of tapes and wires has been successfully demonstrated. Several comments can be made regarding the processing of the conductors:

(1) In the tape-process, the loss of tin can be most effectively reduced by elevating the infiltration temperature to about 850°C.

(2) The isostatic compacting of niobium powder followed by sintering offers a simple approach for achieving a controlled porosity.

(3) A high vacuum in the range $1\text{-}5\times10^{-5}$ mm Hg and a temperature close to 2300°C are required during sintering for the development of essential ductility of the sintered rods.

(4) The filament morphology is strongly dependent on the mode of mechanical deformation employed to reduce the infiltrated rods to wire. Form rolling and wire drawing operations appear to result in a favorable filament structure.

(5) In the present investigation, wires with reduction ratios of approximately 500 or higher require a mere 1 min heat treatment at 950°C for a complete reaction of the tin to form Nb_3Sn filaments.

(6) Protection of the infiltrated core by a tantalum or niobium sheath appears necessary to avoid reaction of the outer copper cladding and the core during heat treatment. In view of the brittle reaction layers formed between monel and the core, the wires with no diffusion barrier should be heat treated for the shortest times and at the lowest temperatures possible. One minute at 930°C seems to be the optimum for the system.

The transition temperature T_c, the critical current density J_c as a function of magnetic field, the magnetization behavior, and the mechanical flexibility of the conductors have been evaluated. The effects of certain important process variables on these properties have also been investigated. From the above study, the following observations can be made with respect to these characteristics:

(1) Zirconium doping is effective in improving the J_c only when the starting niobium powder has been alloyed with it. Alloying the tin bath has no significant effect on the J_c. An addition of 1.5 at.% zirconium to niobium has increased the J_c by more than 50% relative to the undoped conductors at fields above 100 kG.

(2) For a conductor prepared from undoped niobium powder, the superconducting-to-normal transition is sharp ($\Delta T = 0.35°K$) and the mid point T_c is 17.9°K. On the contrary, the doped powder has resulted in a broad transition ($\Delta T = 1.3°K$) and a T_c of 17.2°K.

(3) The T_c decreases with decreasing reaction temperature below 930°C.

(4) Satisfactory agreement at 60-100 kG has been observed between the values of J_c measured by a pulsed field technique and data obtained under steady fields.

(5) Although the times required for a complete reaction at 700-900°C are of the order of hours, the current-carrying capacity of the wires heat treated at these temperatures is as high as those resulting from a short reaction at 950-1000°C. After the formation of Nb_3Sn has been complete, the J_c appears to be fairly insensitive to further increases in the duration of heat treatment at 950°C.

(6) The J_c vs H characteristics deteriorate rapidly when the heat treatment is performed at temperatures above 1000°C.

(7) The current measurements indicate that the J_c increases with decreasing filament thickness down to about 2 μm beyond which there is a tendency toward leveling off.

(8) Coils wound from the wires have hysteresis losses that are independent of the rate of change of field up to about 28 kG/sec. In general, the flux jump stability results are also encouraging.

(9) The minimum diameter to which the wires can be bent without any degradation in the critical currents is 2 cm.

From the various results obtained so far, some optimum conditions would include: (a) copper and tantalum for cladding materials, (b) form rolling and wire drawing to achieve a favorable filament morphology, (c) 1-2 min reaction at 950-1000°C, and (d) Nb_3Sn filament thickness of 1-2 μm. Although more optimization remains to be done with respect to the amount of cladding materials and doping with zirconium, the overall current-carrying capacity of the infiltrated wires is already shown to be superior to the multifilamentary conductors produced by the well developed "bronze approach".

Continuance of the research program appears well warranted and the immediate work should be concerned with the development of continuous lengths of the filamentary wire suitable for testing in a full scale solenoid device. A simple calculation shows that a 2 cm dia×10 cm long sintered rod is needed for a one kilometer wire with a 0.2 mm dia central core. If the cladding materials constitute half the wire cross-section, the final diameter will be 0.283 mm or 0.011 in.

Among other things that need additional work are: (1) an investigation into the mechanism responsible for the J_c degradation in the monel clad wires containing no diffusion barrier, (2) enhancement of the J_c of the wires by means of doping, (3) a better understanding of the magnetization behavior resulting from the interconnected network of filaments and (4) a quantitative estimation of ac losses. Finally, the adaptability of the present powder metallurgy approach to the other technologically important A-15 compounds (e.g., V_3Ga) should be explored.

ACKNOWLEDGEMENTS

The author wishes to thank Dr. M. R. Pickus for his encouragement and guidence throughout the research. The interest shown by Professors E. R. Parker and M. P. Dariel in the project has been a welcome pleasure. The technical help rendered by J. T. Holthius, J. A. Jacobsen and the many people within the Materials and Molecular Research Division is greatly appreciated. I am grateful to Dr. W. S. Gilbert, Dr. F. Voelker, Dr. W. W. Chupp and R. C. Acker at the Accelerator Division of the Lawrence Berkeley Laboratory and Dr. Richard Howard at the Hansen Labs of the Stanford University for their valuable assistance in the conductor evaluation. Thanks are also due to B. V. Narasimha Rao for the transmission electron microscopy, to J. R. Feldman, R. L. Ciardella Dr. J. L. Wang for helpful comments on the manuscript.

This work was performed under the auspices of the U. S. Energy Research and Development Administration through the Materials and Molecular Research Division of the Lawrence Berkeley Laboratory.

REFERENCES

1. B. T. Matthias, Ti Gaballe, S. Geller and E. Corenzwit, Phys. Rev. 95, 1435 (1954).

2. J. E. Kunzler, E. Buchler, F. S. L. Hsu and J. H. Wernick, Phys. Rev. Lett. 6, 89 (1961).

3. M. R. Pickus, V. F. Zackay, E. R. Parker and J. T. Holthius, Intern. J. Powder Met. 9(1), 3 (1973).

4. M. R. Pickus, E. R. Parker and V. F. Zackay, A Method of Making a Ductile Superconductive Material, U. S. Patent 3,815,224, June 11, 1974.

5. B. N. P. Babu, Correlation of Thermo-Mechanically Varied Microstructures with Superconducting Properties of Nb_3Sn Processed by a New Powder Metallurgy Technique (M. S. Thesis), LBL-437, December 1971.

6. T. Tom, Application of Powder Metallurgy Process in the Formation of Nb_3Al Superconductor (M. S. Thesis), LBL-188, December 1971.

7. M. R. Pickus and K. Hemachalam, Materials Science and Engineering 14, 265 (1974).

8. K. Hemachalam and M. R. Pickus, Appl. Phys. Lett. 27, 570 (1975).

9. K. M. Olsen, E. O. Fuchs and R. F. Jack, J. Metals 13, 89 (1961).

10. J. E. Kunzler, Endeavor 23, No. 90 (1964).

11. J. J. Hanak, K. Strater and G. W. Cullen, RCA Reviews 25, 342 (1964).

12. J. J. Hanak, Metallurgy of Advanced Electronic Materials G. E. Brook, ed. (Interscience Publishers, NY, 1963), p. 161.

13. D. L. Martin, M. G. Benz, C. A. Bruch and C. H. Rosner, Cryogenics 3, 161 (1963).

14. M. G. Benz, G. E. Reports, No. 66-C-044 (1966).

15. D. Koch, H. Speidel, G. Otto and E. Saur, Z. Physik 180, 476 (1964).

16. T. L. Chu and J. R. Gaveler, J. Electrochem. Soc. 113, 1289 (1966).

17. K. Tachikawa and S. Fukuda, Trans. Nat. Research Inst. Metals 9, 39 (1967).

18. K. Tachikawa, Proc. Appl. Superconductivity Conf., Annapolis, May 1972, IEEE Pub. New York, p. 371.

19. A. R. Kaufman and J. J. Pickett, Bull. Am. Phys. Soc. 15, 838 (1970), J. Appl. Phys. 42, 58 (1971).

20. M. Suenaga and W. B. Sampson, Appl. Phys. Lett. 18, 584 (1971).

21. M. Suenaga and W. B. Sampson, Appl. Phys. Lett. 20, 443 (1972).

22. J. E. Crow and M. Suenaga, Proc. Appl. Superconductivity Conf., Annapolis, May 1972, IEEE Pub. New York, p. 472.

23. M. Suenaga and W. B. Sampson, ibid, p. 481.

24. R. M. Scanlan and W. A. Fietz, Proc. Appl. Superconductivity Conf., Argonne, 1974, IEEE Trans. on Magnetics, Vol. Mag-11 (1975), p. 289.

25. E. Gregory, W. C. Marancik and F. T. Ormand, ibid, p. 295.

26. D. C. Larbalestier, P. E. Madsen, J. A. Lee, M. N. Wilson, J. P. Charlesworth, ibid, p. 247.

27. W. D. Coles, 4th Intern. Conf. on Magnet Technology, Brookhaven National Laboratory, Sept. 1972.

28. P. H. Brisbin and W. D. Coles, Proc. Appl. Superconductivity Conf., Argonne, 1974, IEEE Trans. on Magnetics, Vol. Mag-11 (1975), p. 283.

29. C. C. Tsuei and L. R. Newkirk, J. Mat. Sci. 8, 1307 (1973).

30. C. C. Tsuei, J. Appl. Phys. 45, 1385 (1974).

31. C. C. Tsuei, M. Suenaga and W. B. Sampson, Appl. Phys. Lett. 25, 318 (1974).

32. M. G. Benz, Trans. Met. Soc. AIME 242, 1067 (1968).

33. M. Suenaga, T. S. Lahman and W. B. Sampson, J. Appl. Phys. 45, 4049 (1974).

34. P. F. Smith, J. D. Lewin, C. R. Walters, M. N. Wilson and A. H. Spurway, J. Phys. D. Appl. Phys. 3, 1517 (1970).

35. W. B. Sampson, R. B. Britton, P. F. Dahl, A. D. McInturff, G. H. Morgan and K. E. Robins, Particle Accelerators 1, 173 (1970).

36. R. Hancox, Phys. Lett. 16, 208 (1965).

37. R. Hancox, IEEE Trans. Magnetics 4, 456 (1968).

38. R. Ciardella, private communication.

39. M. L. Picklesimer, United States Atomic Energy Commission, Oak Ridge National Laboratory Report 2296 (1957).

40. R. M. Scanlan, W. A. Fietz, E. F. Koch, J. Appl. Phys. 46, 2244 (1975).

41. Schawlow and Delvin, Phys. Rev. 113, 120 (1959).

42. J. Chabanne, Effect of the Microstructure on the Superconductive Properties of Nb_3Sn in a NbC Matrix (M. S. Thesis), UCRL 17826, September 1967.

43. T. N. Garrett, Pulsed Magnetic Fields and the Critical Current Densities of Superconducting Nb_3Sn Strips in these Fields (M. S. Thesis), LBL-448, December 1971.

44. W. Gilbert, F. Voelker, R. Acker and J. Kaugerts, Proc. Appl. Superconductivity Conf., Annapolis, Maryland (1972), p. 486. Also, LBL-571.

45. T. H. Courtney, G. W. Pearsall and J. Wulff, Trans. Met. Soc. AIME 233, 212 (1965).

46. R. Enstrom, T. Courtny, G. Pearsall and J. Wulff, Metallurgy of Advanced Electronic Materials, G. E. Brock, ed. (Interscience Publishers, NY, 1962), p. 121.

47. T. B. Reed and H. C. Gatos, J. Appl. Phys. 33, 2657 (1962).

48. J. J. Hanak, G. D. Cody, P. R. Aron and H. C. Hitchcock, High Magnetic Fields, Lax, et al., ed. (Wiley, NY, 1961), p. 353.

49. R. D. Blaugher, R. A. Hein, J. E. Cox and R. M. Waterstrat, J. Low Temp. Phys. 1, 531 (1969).

50. T. B. Reed, H. G. Gatos, W. J. LaFleur and T. J. Roddy, Metallurgy of Advanced Electronic Materials, G. E. Brock, ed. (Interscience Publishers, NY, 1962), p. 71.

51. H. R. Hart, Jr., I. S. Jacobs, C. L. Kolbe and P. E. Lawrence, High Magnetic Fields (John Wiley and Sons, NY, 1962), p. 584.

52. R. B. Flippen, Phys. Rev. 137, 1822 (1965).

53. H. Bell, Y. M. Shy, D. E. Anderson and L. E. Toth, J. Appl. Phys. 39, 2797 (1968).

54. K. Inoue and K. Tachikawa, Trans. of Nat. Res. Inst. for Metals 13, 305 (1971).

55. J. P. Charlesworth, I. Macphail and P. E. Madsen, J. Mat. Sci. 5, 580 (1970).

56. J. D. Livingston, Proc. Summer Study on Superconducting Devices and Accelerators, A. G. Prudell, ed. (Brookhaven, 1968), p. 377.

57. E. J. Kramer, J. Appl. Phys. 44, 1360 (1973).

58. W. W. Webb, Proc. Summer Study on Superconducting Devices and Accelerators, A. G. Prudell, ed. (Brookhaven, 1968), p. 396.

59. D. Dew-Hughes, Phil. Mag. 30, 293 (1974).

60. J. Sutton and C. Baker, Phys. Lett. 21, 601 (1966).

61. Produced by Airco, Inc., Murray Hill, NJ.

62. M. Suenaga, W. B. Sampson and C. J. Klamut, Proc. Appl. Superconductivity Conf., Argonne, 1974, IEEE Trans. on Magnetics, Vol. Mag-11 (1975), p. 231.

63. R. Randall, J. Wong, D. W. Deis, B. J. Shaw and M. R. Daniel, ibid, p. 291.

Table I. Sieve and sub-sieve analysis of niobium powder.

Sieve	Particle Size (μm)	Distribution (%)
-270+325	53-44	2
-325+400	44-37	26
-400+500	37-30	18
-500+750	30-20	18
-750+1000	20-15	18
-1000	<15	18

Table II. Thermo-mechanical history of powder-rolled tapes.

Tape Designation	Powder Composition	Infiltrant Composition and Temp.	Mechanical Reduction	Diffusion Environment	Approximate Nb_3Sn Vol. Fraction
1	Nb	Sn 650°C	Room Temp.	Sn	30%
2	Nb	Sn 650°C	-72°C	Sn	40%
3	Nb	Sn 850°C	Room Temp.	Sn	50%
4	Nb	Sn-1.5 at.% Zr	Room Temp.	Sn-1.5 at.% Zr	34%
5	Nb-1.5 at.% Zr	800°C*	Room Temp.	He	36%

Common things for all tapes: Powder size: <44 μm; vacuum sintering at 2100±20°C for 3-4 min; % mechanical reduction: 75-80; heat treatment at 970 10°C for 5 min.

*The higher infiltration temperature was necessary for wetting.

FIGURE CAPTIONS

Fig. 1. Equilibrium phase diagram of niobium-tin system.

Fig. 2. Porous niobium tape infiltrated with tin (a) at 650°C and (b) at 850°C. Phase identification: white-tin; grey-niobium; dark-Nb_6Sn_5.

Fig. 3. Longitudinal sections of tapes reacted at 970°C for 5 min; (a) infiltrated at 650°C and rolled at room temperature (b) infiltrated at 650°C and rolled at -72°C, and (c) infiltrated at 850°C and rolled at room temperature. Phase identification: white-unreacted tin; grey-niobium; dark-Nb_3Sn.

Fig. 4. Typical cross section of reacted tape.

Fig. 5. Schematic diagram of filamentary wire fabrication process.

Fig. 6. Schematic diagram of Abar furnace; 1. extension tube, 2. tantalum rod, 3. back filling port, 4. electrical leads, 5. heating element, 6. niobium specimen, 7. radiation shields, 8. water cooled wall, 9. W-5% Re vs W-26% Re thermocouple point, 10. vacuum connection, 11. quartz tube, 12. graphite crucible, 13. liquid tin bath and 14. resistance heater.

Fig. 7. Tin-infiltrated niobium rods made by pressureless sintering of (a) -325+400 mesh Nb and (b) -400 mesh Nb.

Fig. 8. Infiltrated rods made by isostatic compaction and sintering of (a) -270 mesh Nb and (b) -270+325 mesh Nb.

Fig. 9. Cross sections of heat treated wires reduced by (a) swaging only; (b) form rolling followed by wire drawing and (c) wire drawing only.

Fig. 10. Form rolling mill.

Fig. 11. Wire drawing bench.

Fig. 12. Cross sections of wires clad with monel alone; (a) before heat treatment; (b) after 3 min at 900°C and (c) 1 min at 930°C.

Fig. 13. Cross sections of multicore wires containing (a) 6 tantatum cladd infiltrated cores around a central copper core and (b) 7 in. filtrated cores in monel with no tantalum barrier. The outer sheath is monel in both.

Fig. 14. Schematic of the circuitry used for inductive measurement of transition temperature.

Fig. 15. Probes with specimens in place for measuring (a) critical currents in steady fields, (b) critical currents in pulsed fields and (c) magnetization behavior.

Fig. 16. (a) Pulse magnet and (b) a schematic representation pf of pulsed field apparatus for critical current measurements.

Fig. 17. Typical oscilloscope facings of sample current, sample voltage and magnetic field.

Fig. 18. Block diagram of magnetization setup.

Fig. 19. Variation of transition temperature with the reaction temperature.

Fig. 20. A comparison of the superconducting transition of conductors made from undoped niobium and niobium doped with 1.5 at.% zirconium.

Fig. 21. Critical current density of the core as a function of magnetic field under pulsed and steady field conditions.

Fig. 22. Pulsed field dependence of critical current density of Tapes 1, 2 and 3 which correspond to the micrographs (a), (b) and (c) respectively of Fig. 3.

Fig. 23. Pulsed field dependence of critical current density of Tapes 4 and 5. 1.5 at.% Zr was added to the tin in Tape 4 and to the niobium in Tape 5. Tape 1 is plotted for comparison.

Fig. 24. Influence of deformation mode on the critical current density of the core (J_c) as a function of pulsed field (H).

Fig. 25. Typical (a) longitudinal and (b) cross sectional micrographs of reacted wire with 0.3 mm dia core

Fig. 26. J_c vs H characteristics for 0.3 mm-dia core wire reacted for different times at 800°C.

Fig. 27. J_c vs H characteristics for 0.3 mm-dia core wire reacted for different times at 950°C.

Fig. 28. Transmission electron micrographs showing Nb_3Sn grains of specimens reacted at 950°C for (a) 2 min and (b) 30 min.

Fig. 29. J_c vs H characteristics of 0.3 mm-dia core wire reacted for 2 min at different temperatures.

Fig. 30. J_c of 0.3 mm-dia core wire at 50, 100 and 150 kG as a function of reaction temperature.

Fig. 31. J_c vs H characteristics of wires with varying core sizes.

Fig. 32. J_c as a function of reduction ratio (and N_3Sn filament size).

Fig. 33. Submicron porosity resulting from the formation of Nb_3Sn at 950°C; (a) 0.22 mm dia core reacted for 2 min (b) 0.3 mm dia core reacted for 2 min (c) 0.3 mm dia core reacted for 15 min and (d) 0.4 mm dia core reacted for 8 min.

Fig. 34. Pulsed field dependence of the critical current density in the 6 infiltrated cores of a multicore conductor.

Fig. 35. Cross sectional micrographs of (a) tantalum and monel clad infiltrated wire (b) monel clad infiltrated wire and (c) commercial multifilamentary Nb_3Sn wire.

Fig. 36. Pulsed field dependence of the overall critical current density (i.e., for the entire cross section) of three wires. Curves 1, 2 and 3 correspond to the wires whose cross sections are shown in (a), (b) and (c) respectively of Fig. 35.

Fig. 37. Typical magnetization tracings.

Fig. 38. Hysteresis loss of wire with 0.3 mm dia core as a function of rate of change of field for different values of peak field.

Fig. 39. Hysteresis loss as a function of peak field for two wires with 0.22 mm dia and 0.33 mm dia cores.

Fig. 40. Degradation of current-carrying capacity with bending diameter for three infiltrated wires.

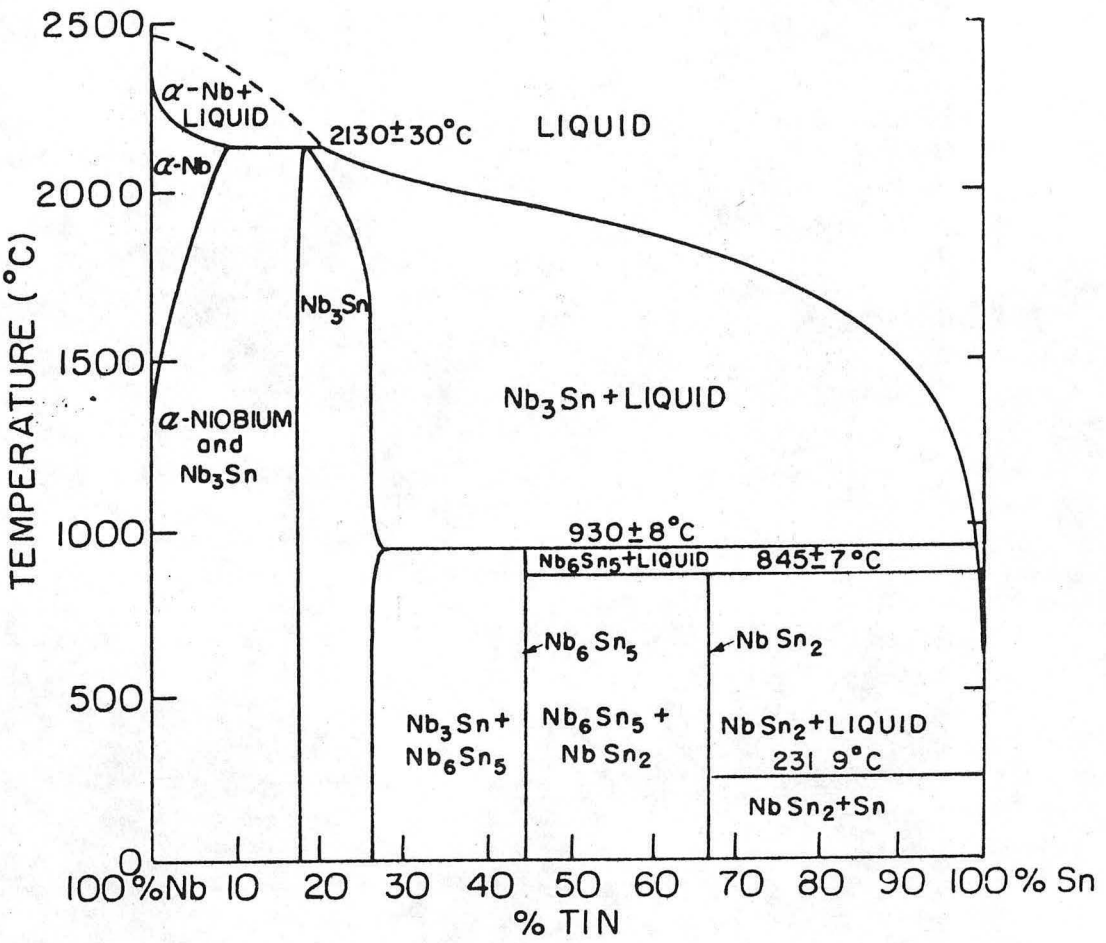

XBL 7110-7515A

Fig. 1

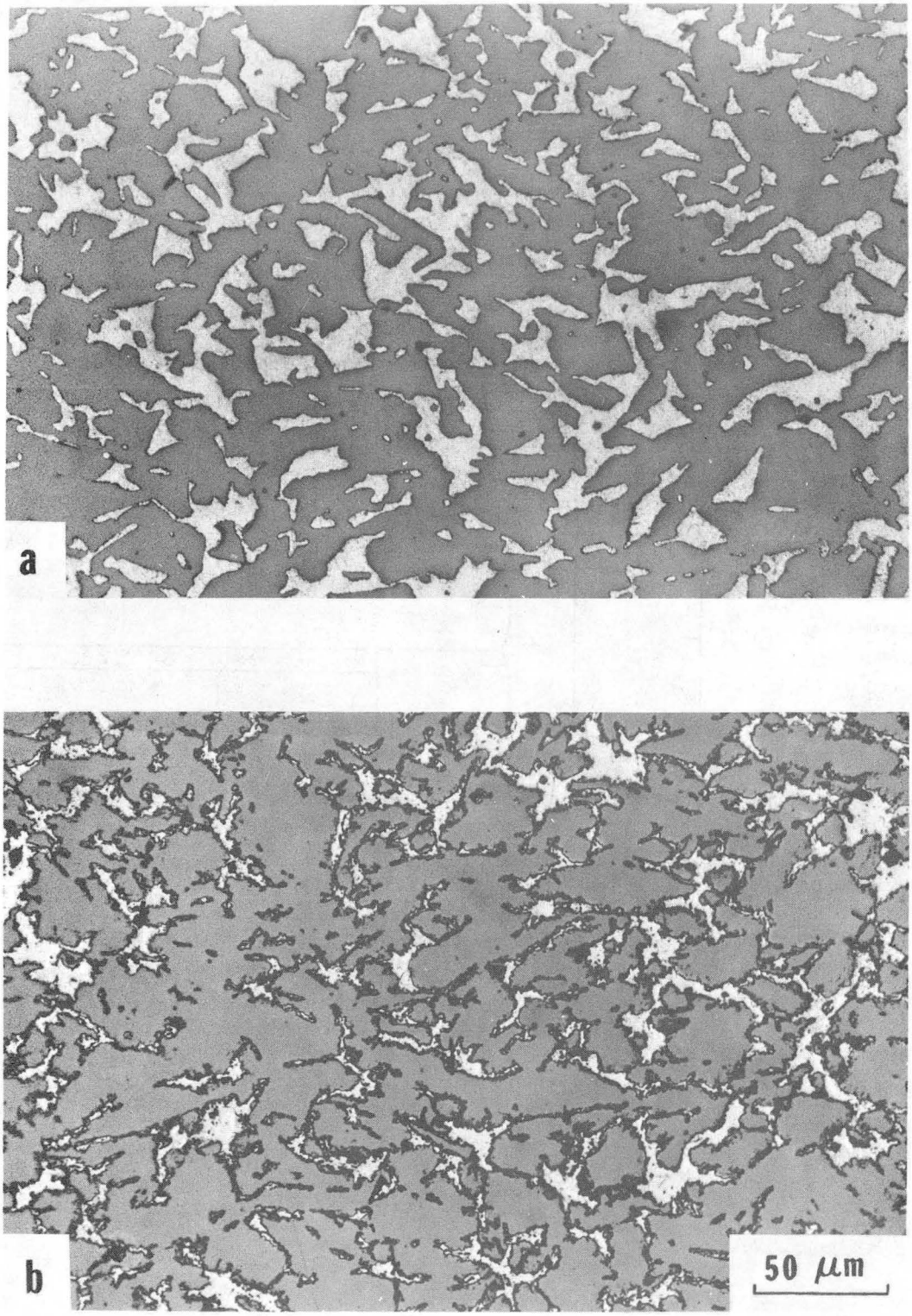

XBB 7512-9129

Fig. 2

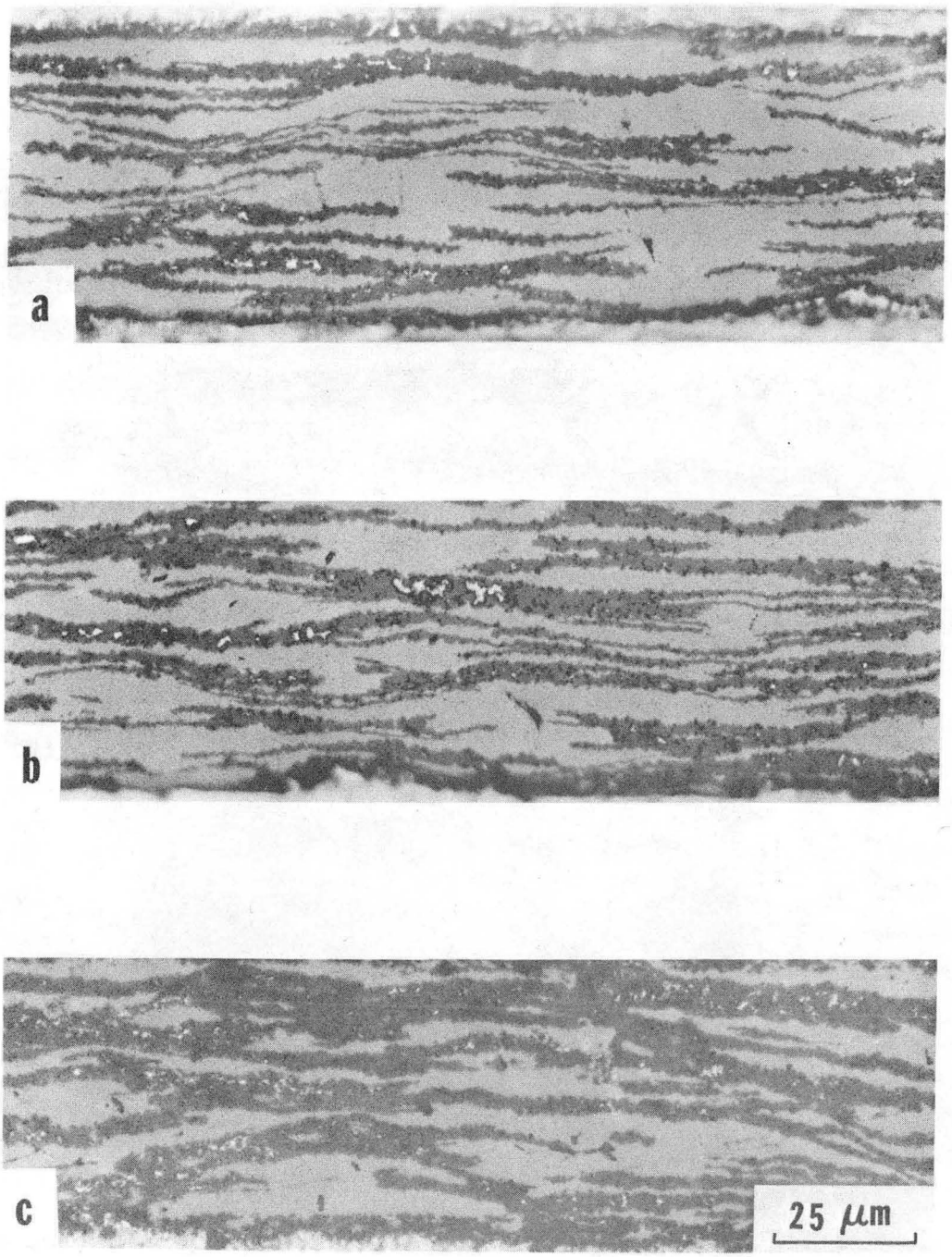

XBB 7512-9122

Fig. 3

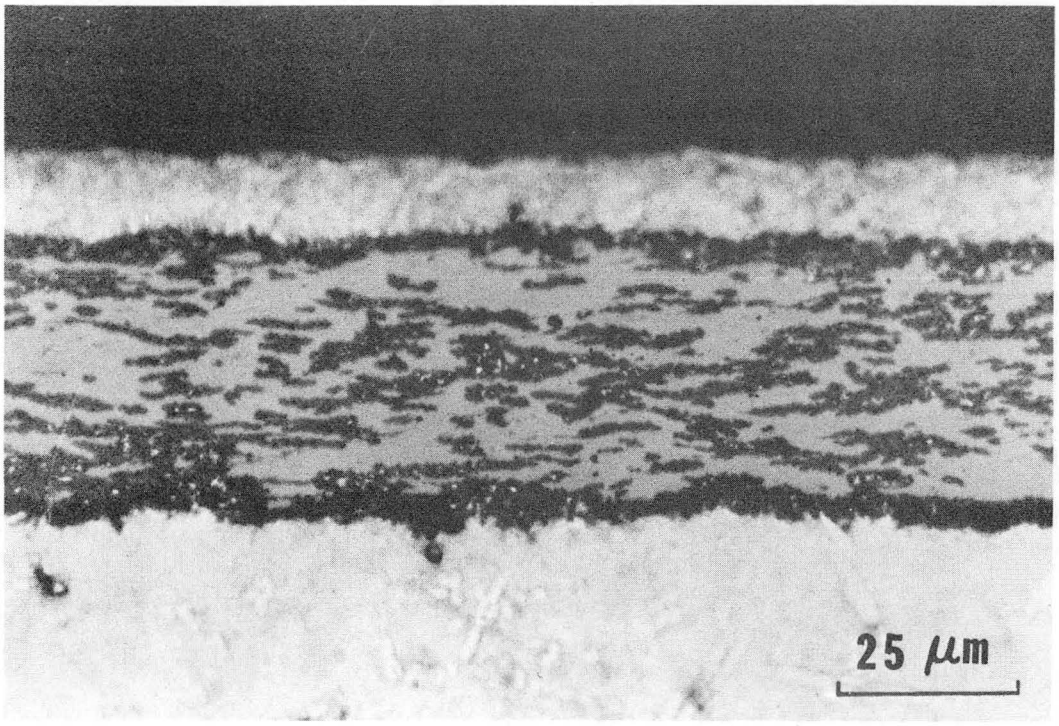

XBB 7512-9120

Fig. 4

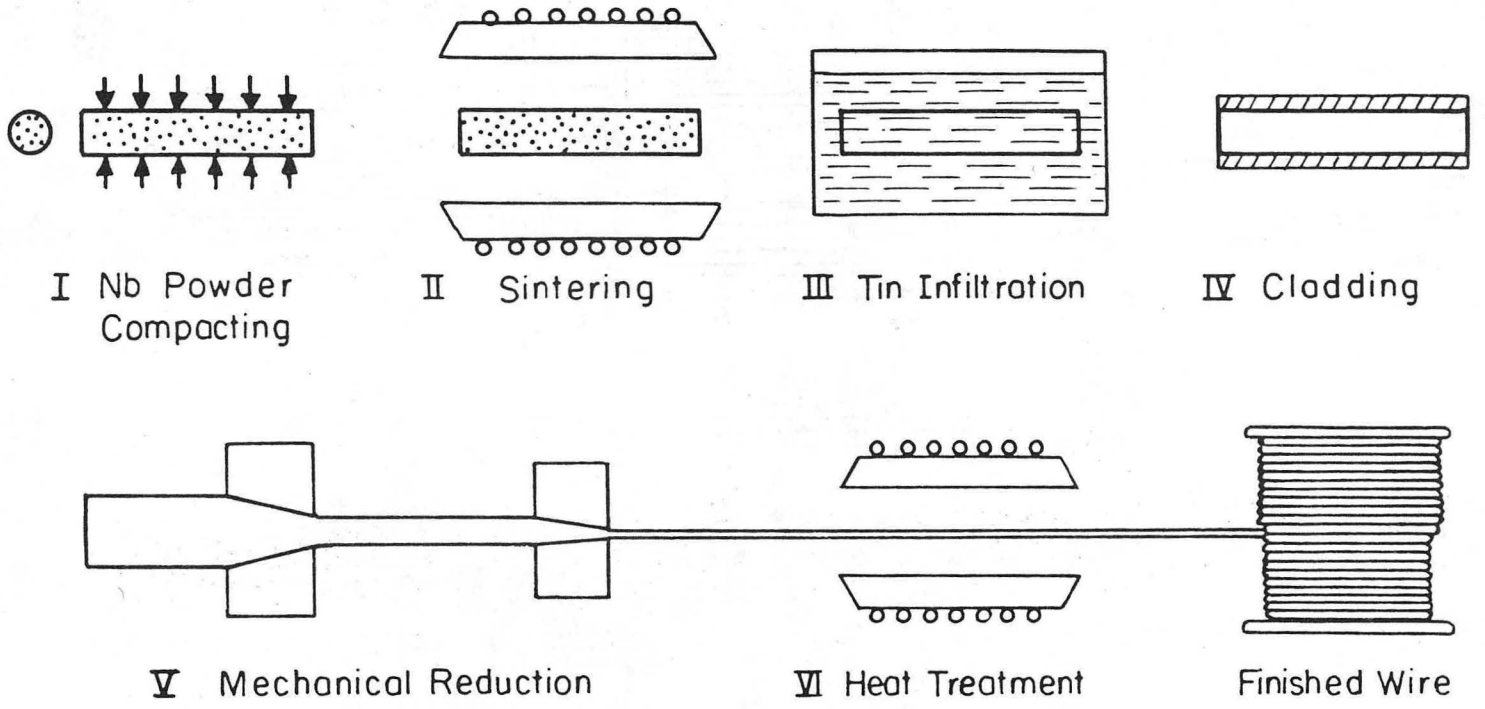

Fig. 5

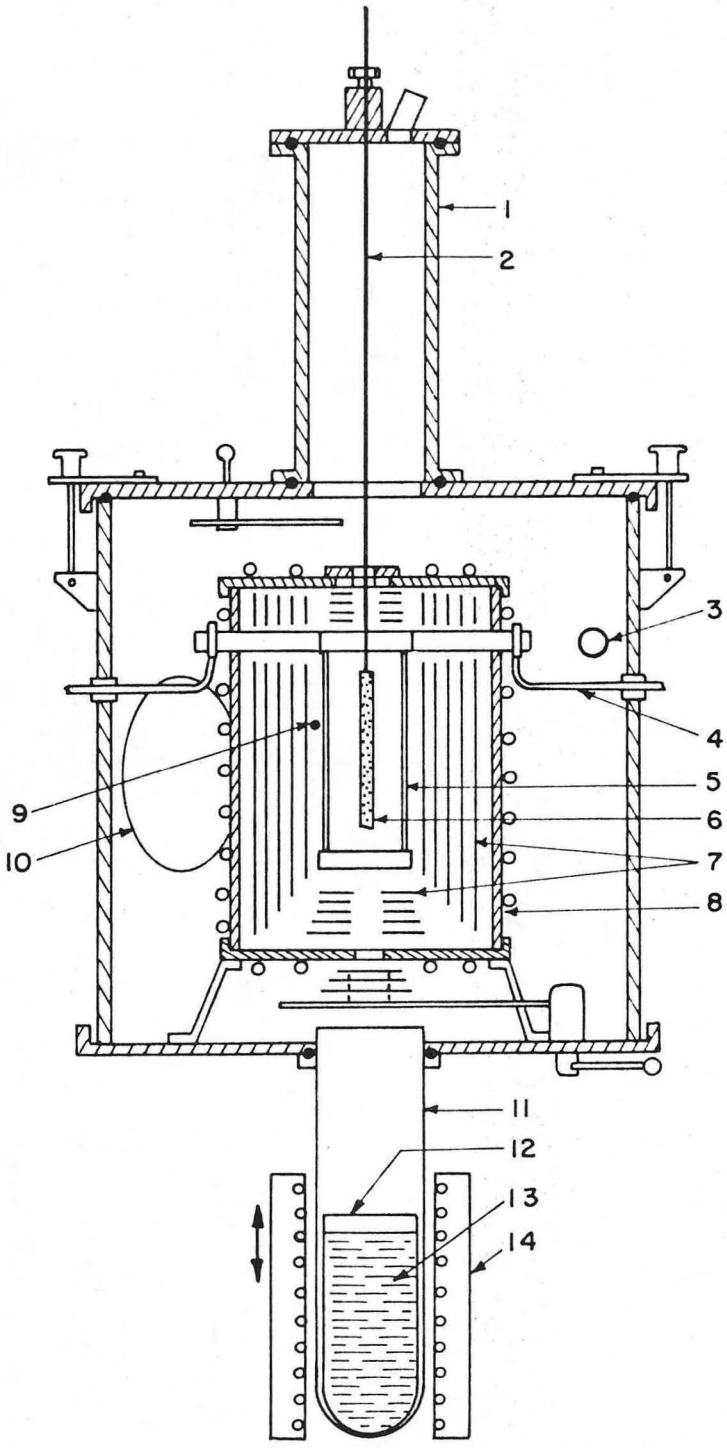

XBL 7210-7043

Fig. 6

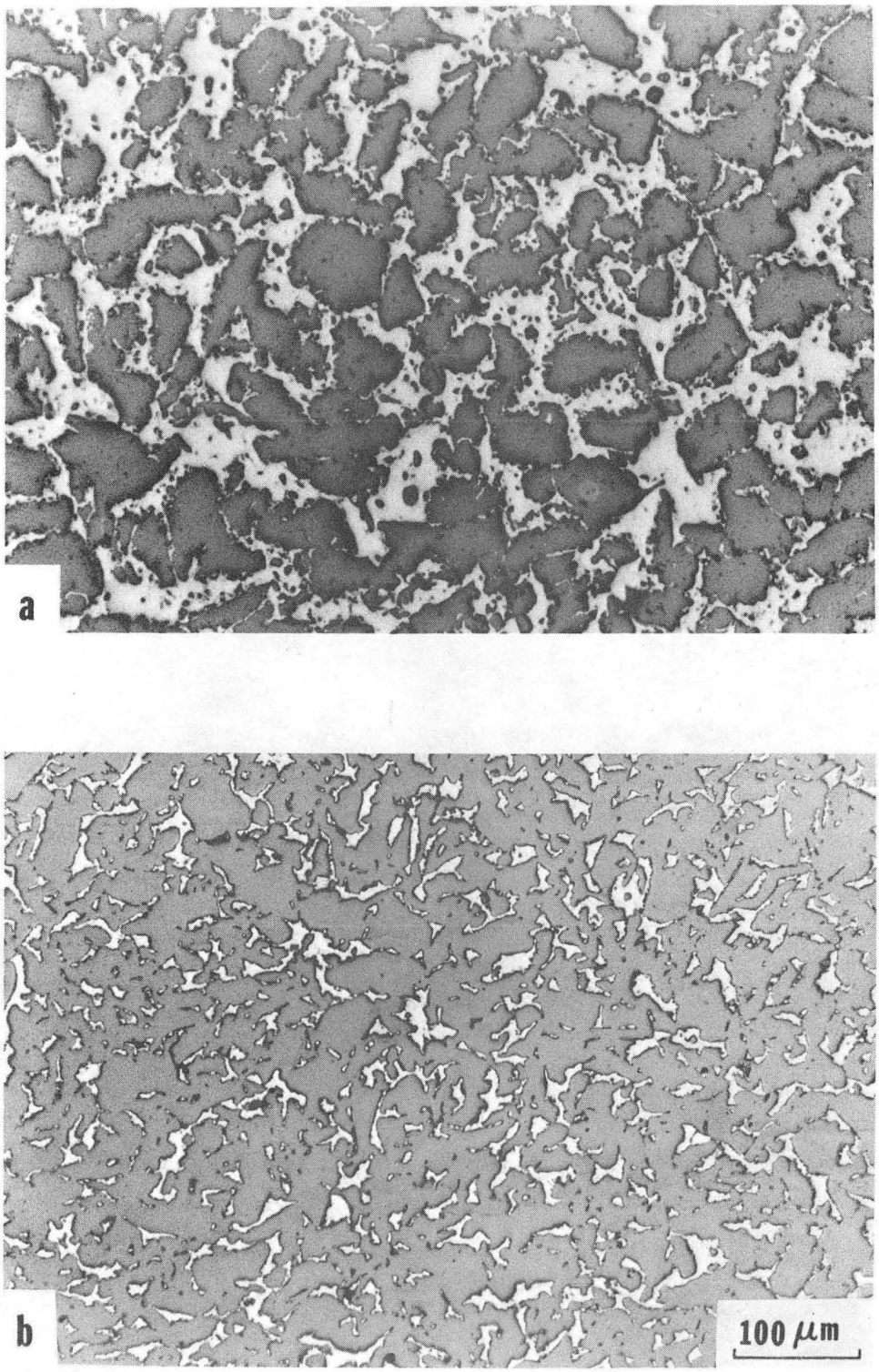

XBB 7512-9130

Fig. 7

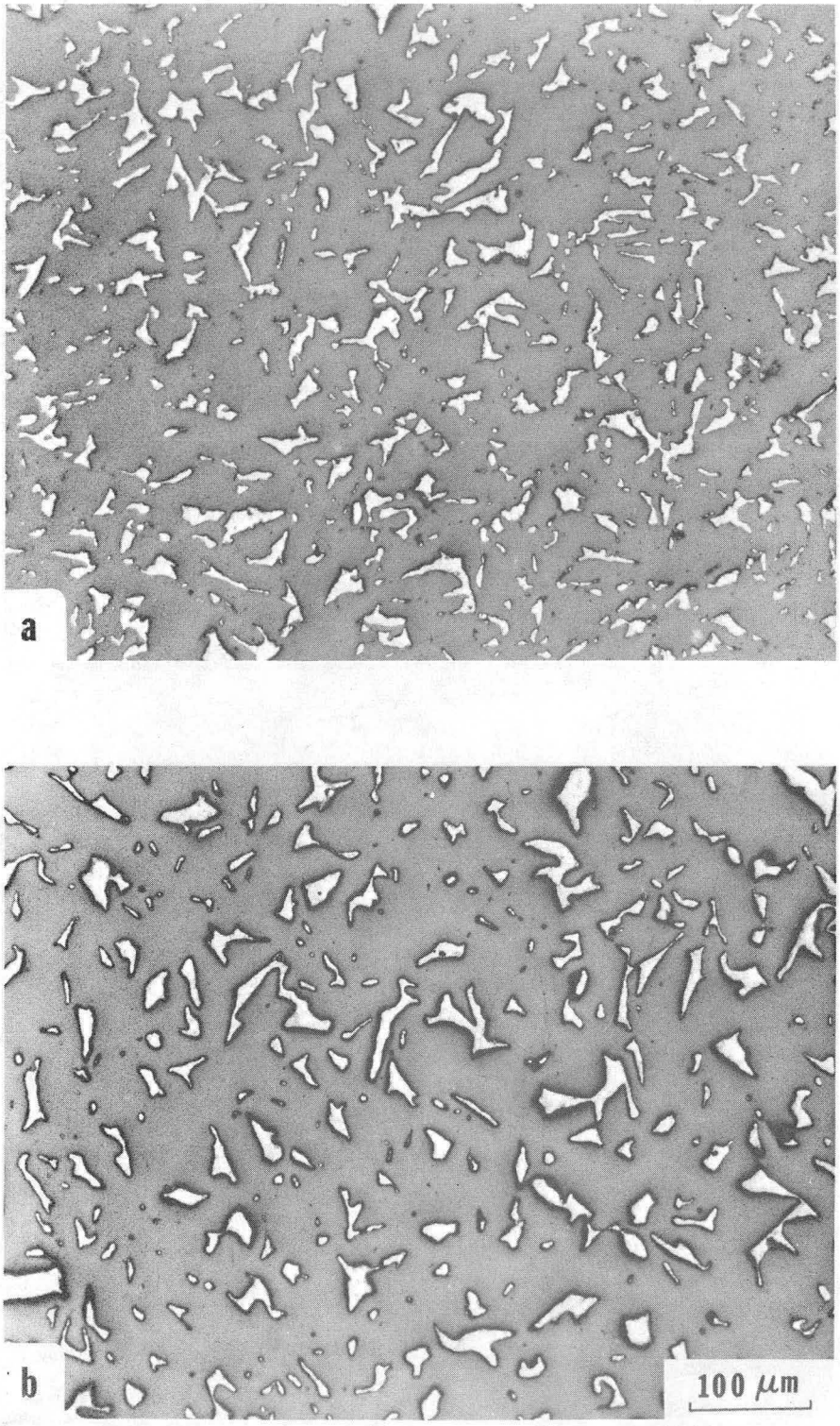

XBB 7512-9131

Fig. 8

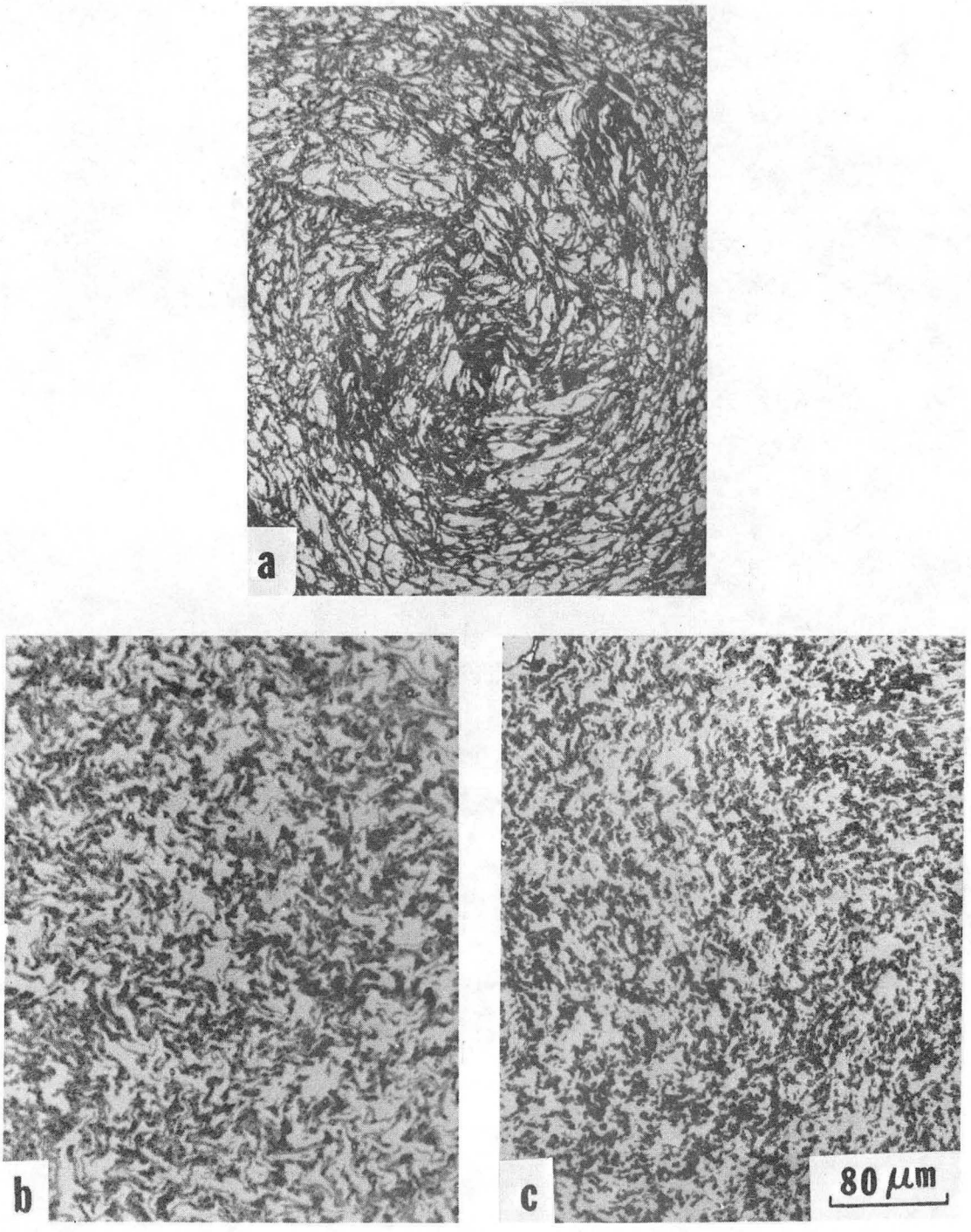

XBB 7512-9127

Fig. 9

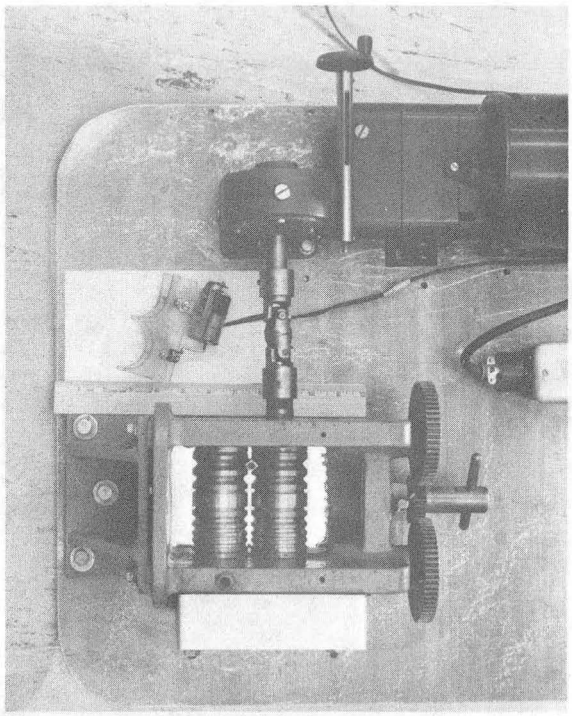

Fig. 10

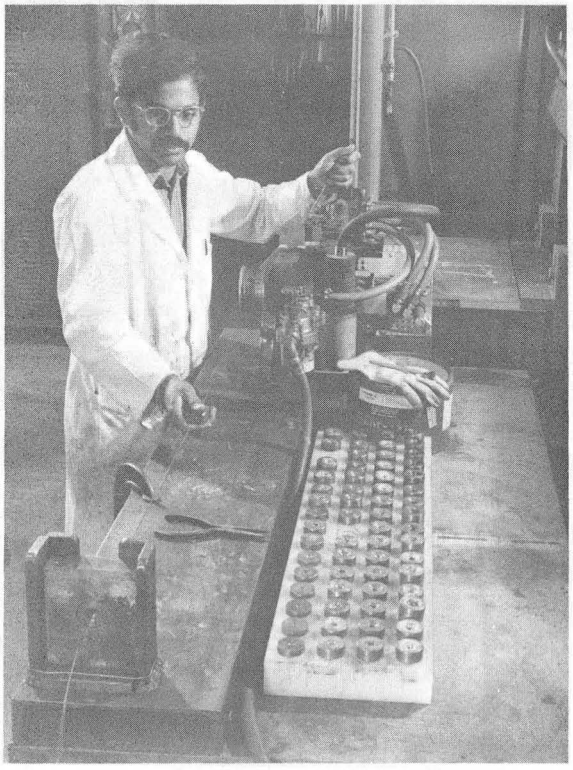

XBB 758-6507A

Fig. 11

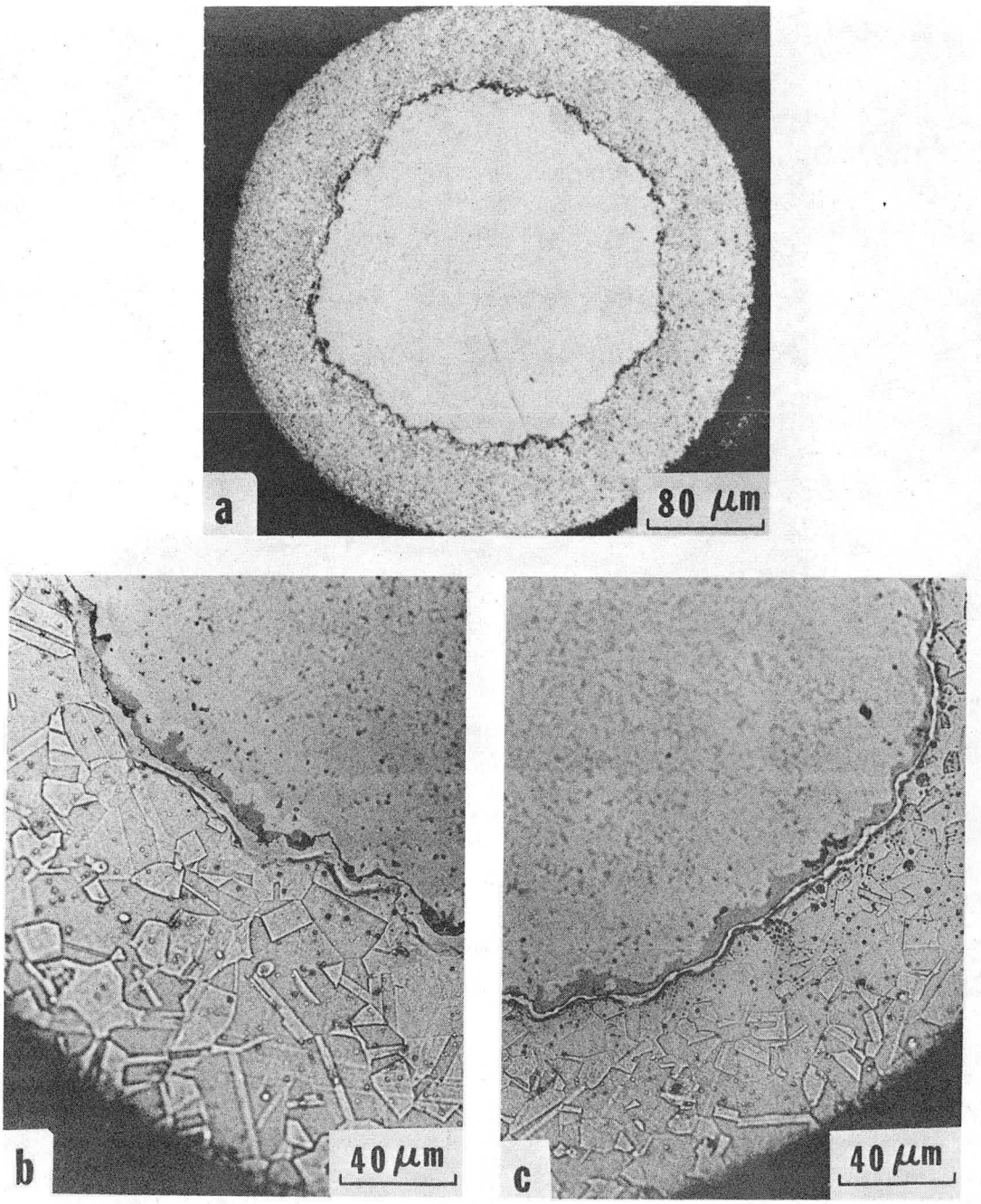

XBB 7512-9123

Fig. 12

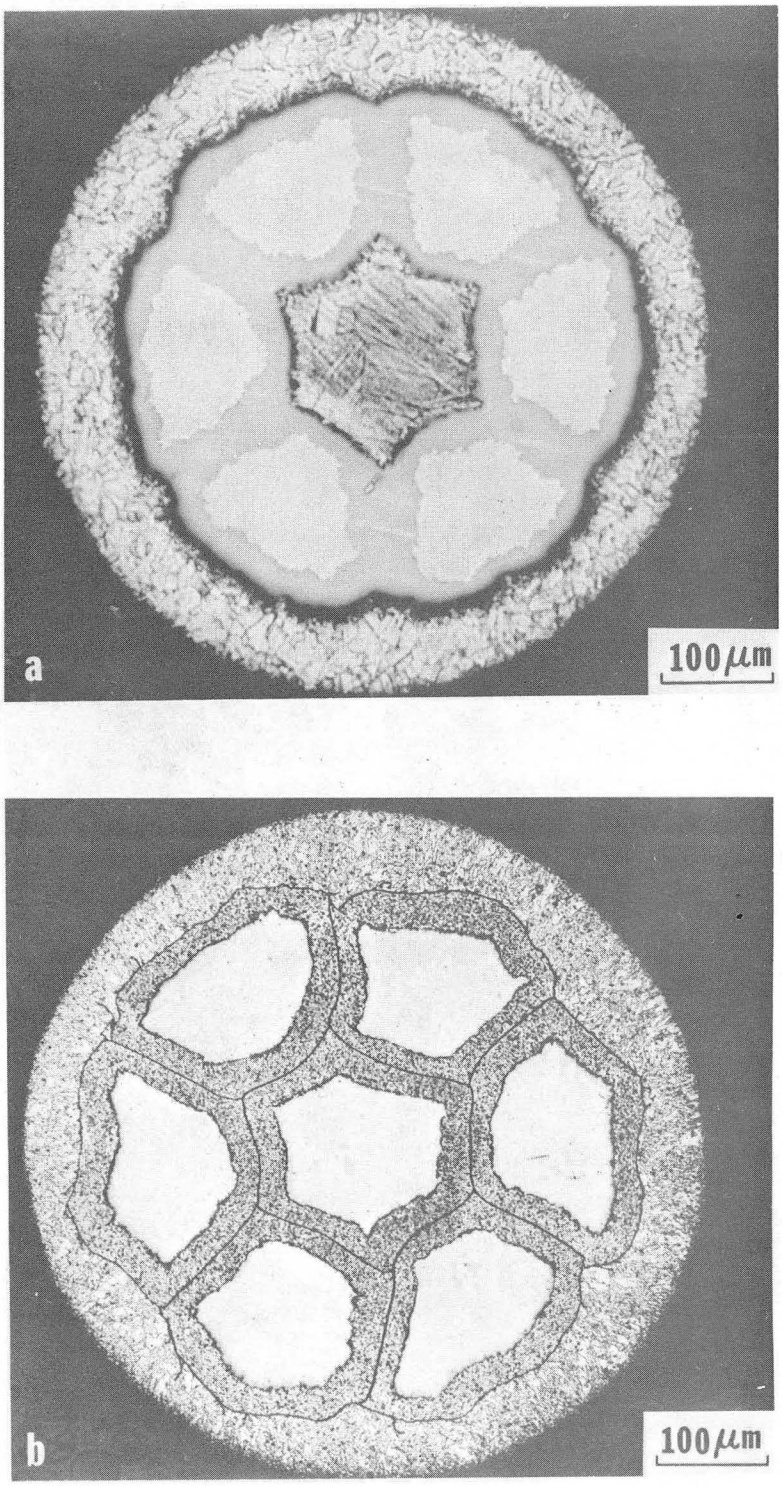

XBB 7512-9121

Fig. 13

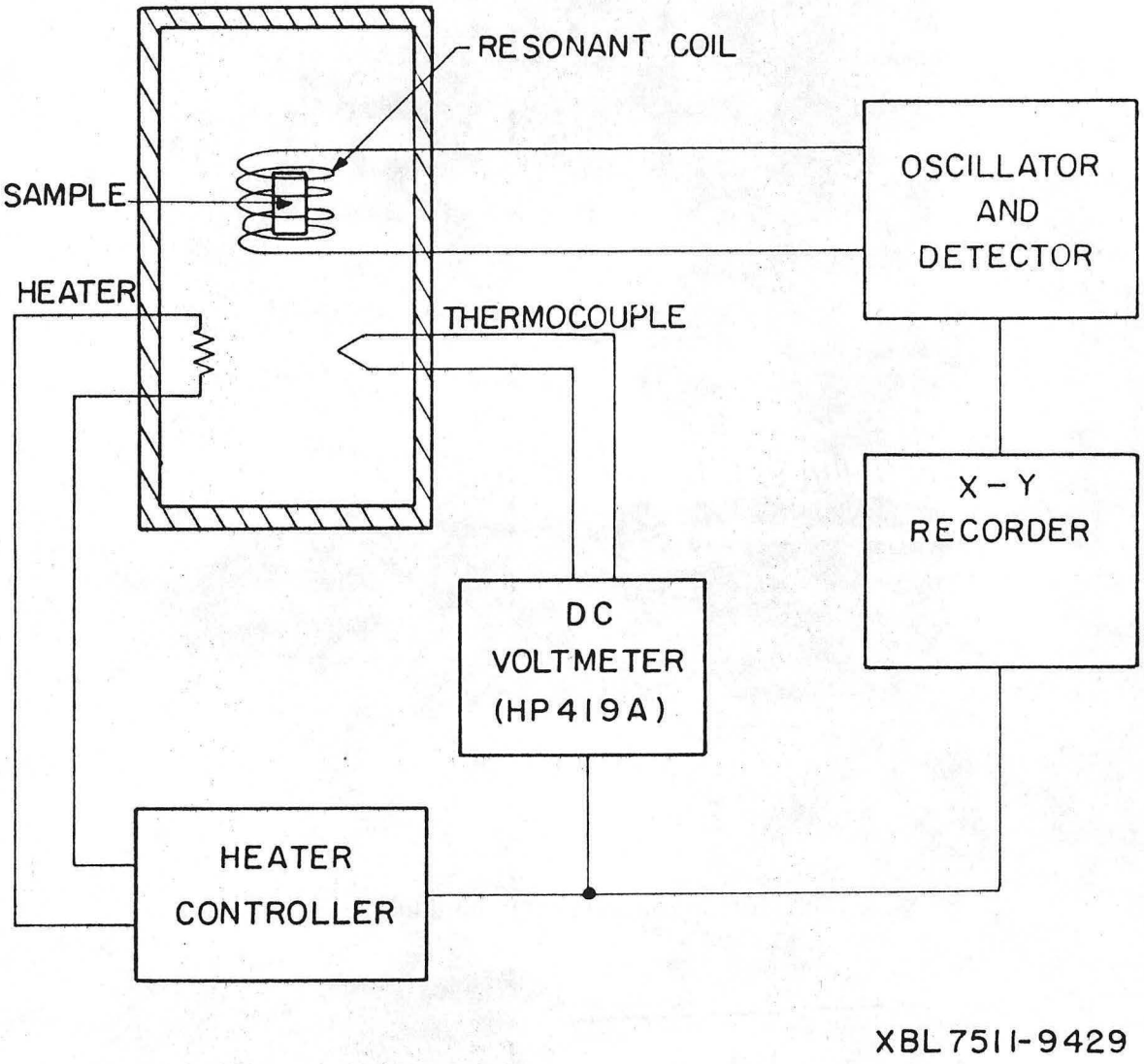

Fig. 14

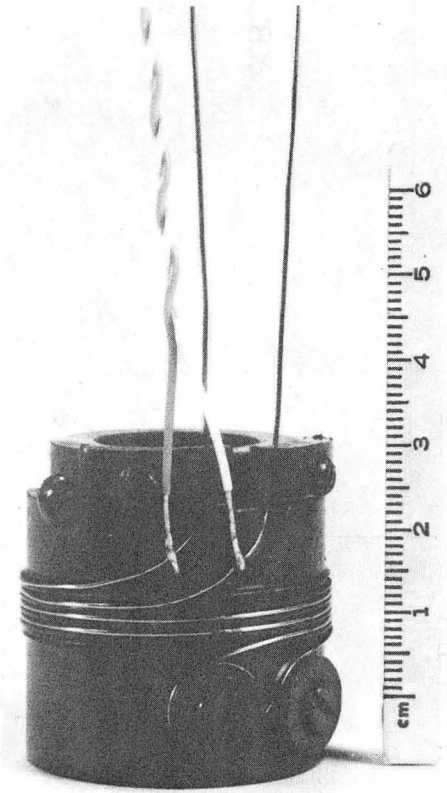

a

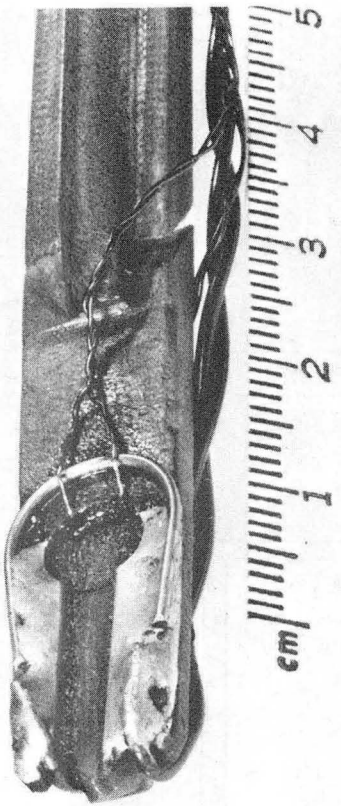

b

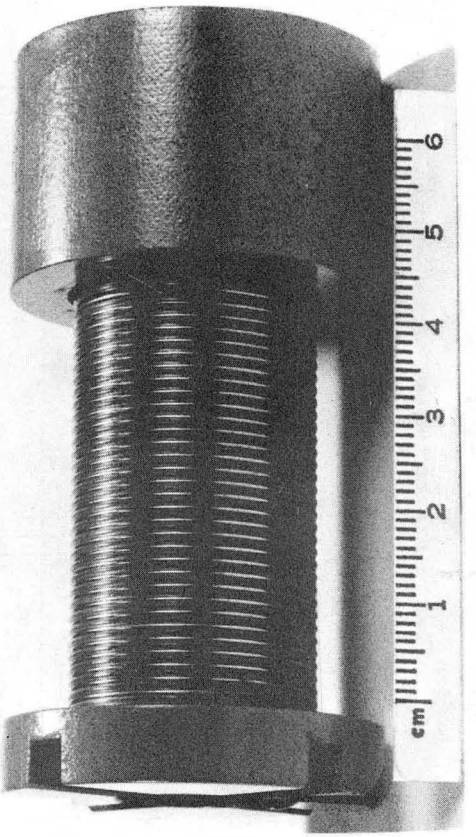

c

XBB 7512-9119

Fig. 15

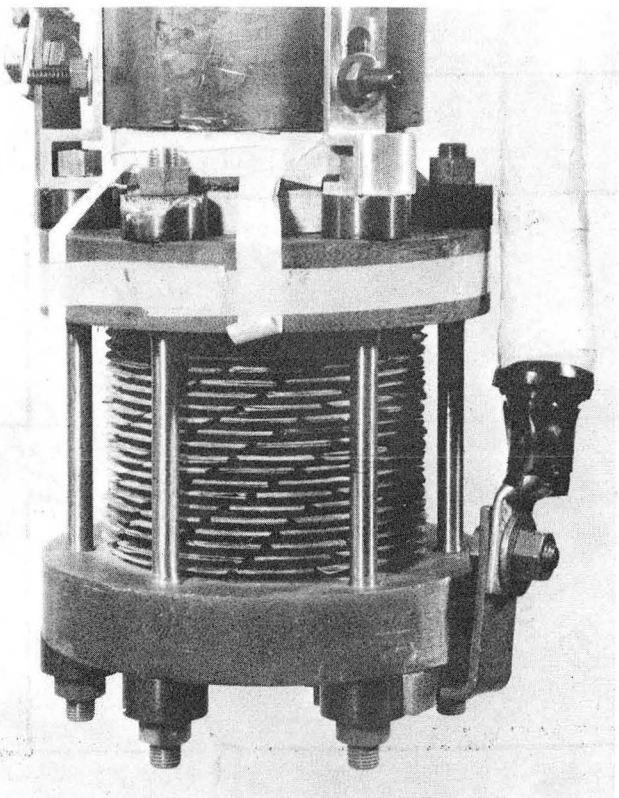

a

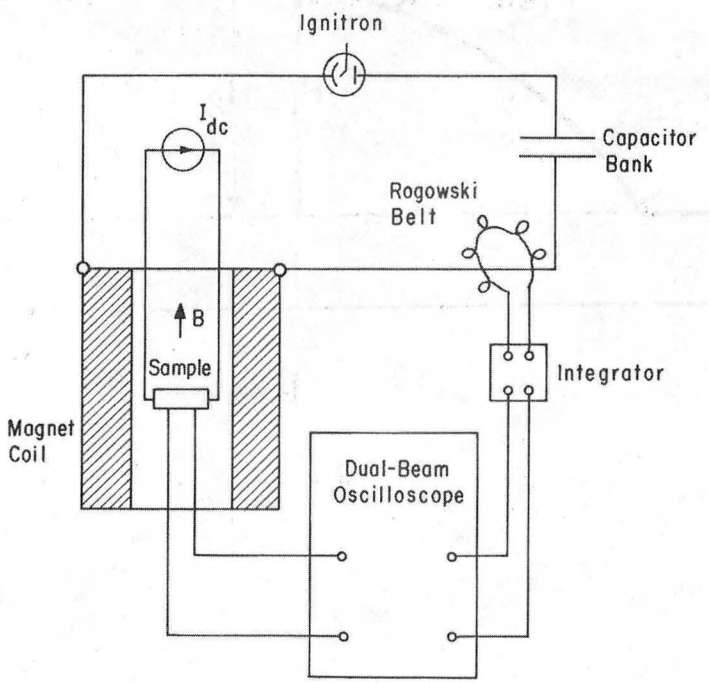

b

XBB 7112-5960A

Fig. 16

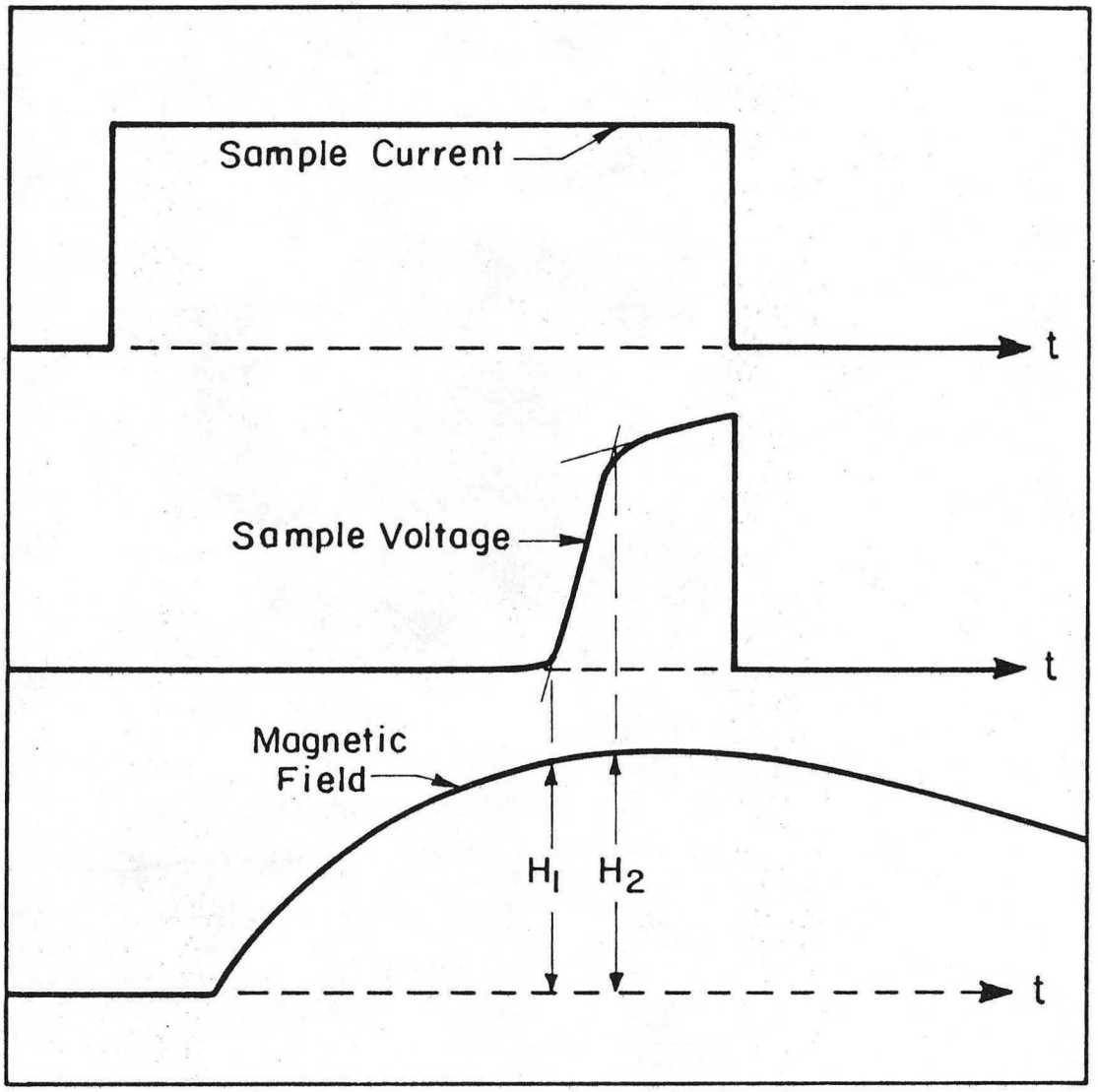

XBL 7512-9475

Fig. 17

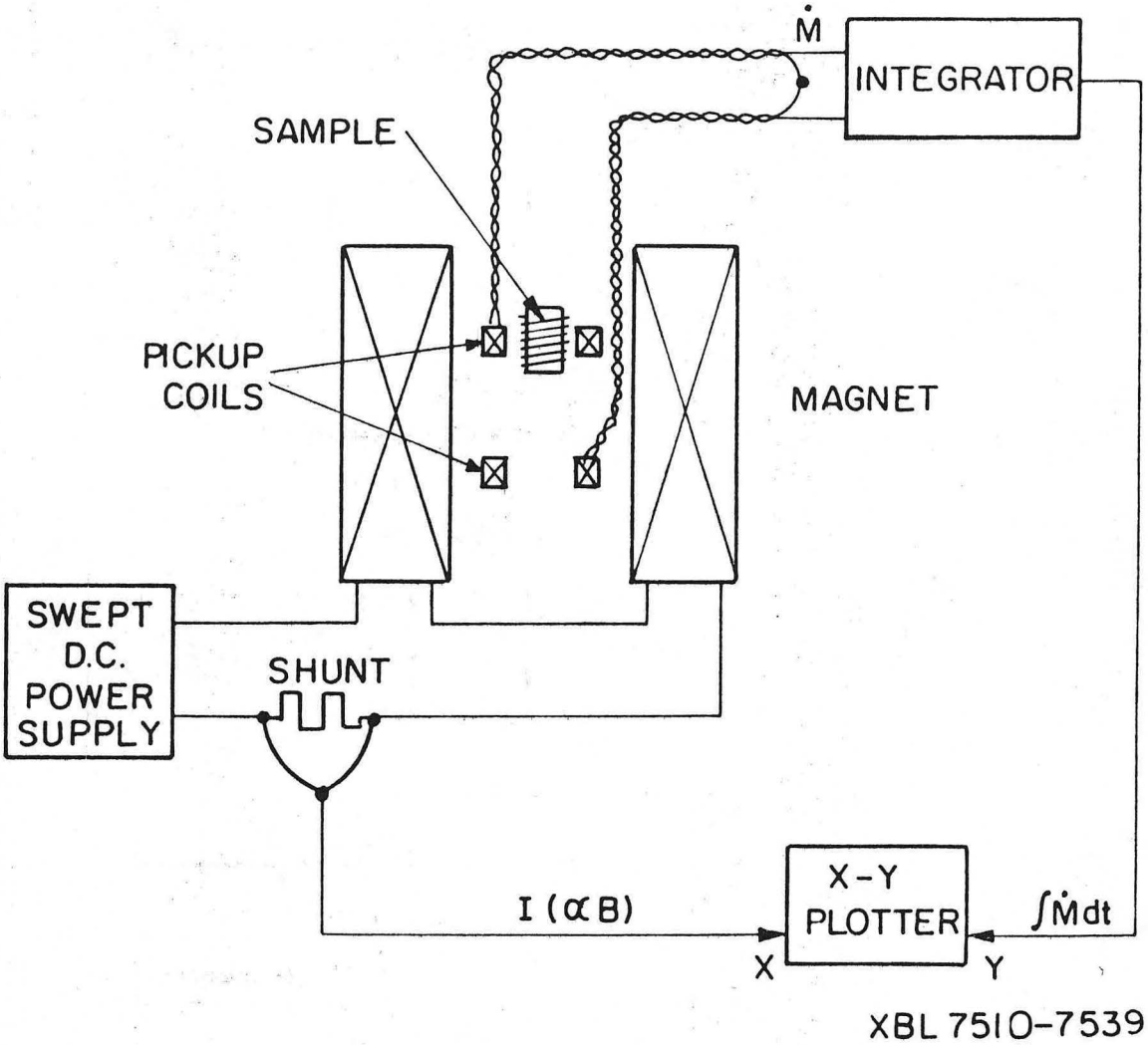

Fig. 18

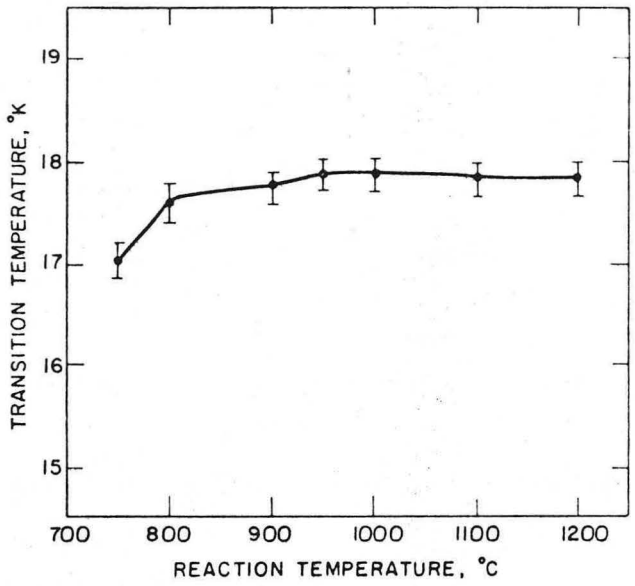
TRANSITION TEMPERATURE, °K
19
18
17
16
15
700
800
900
1000
1100
1200
REACTION TEMPERATURE, °C

Fig. 19

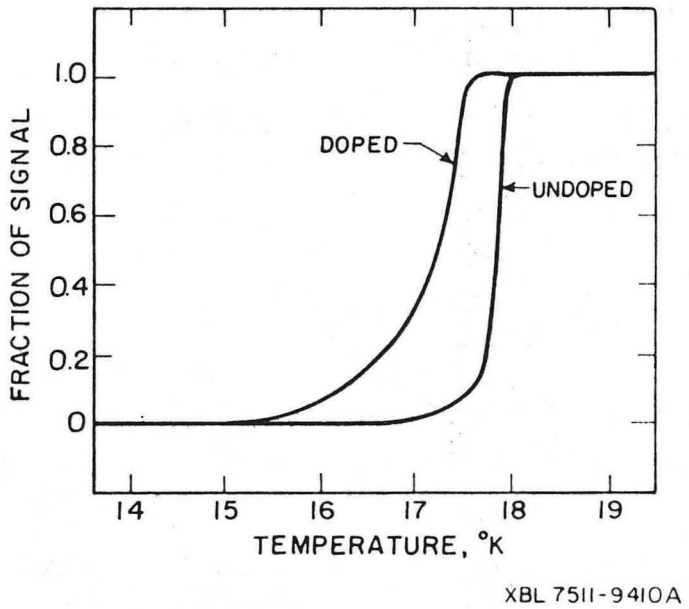
FRACTION OF SIGNAL
1.0
0.8
0.6
0.4
0.2
0
DOPED
UNDOPED
14
15
16
17
18
19
TEMPERATURE, °K
XBL 7511-9410A

Fig. 20

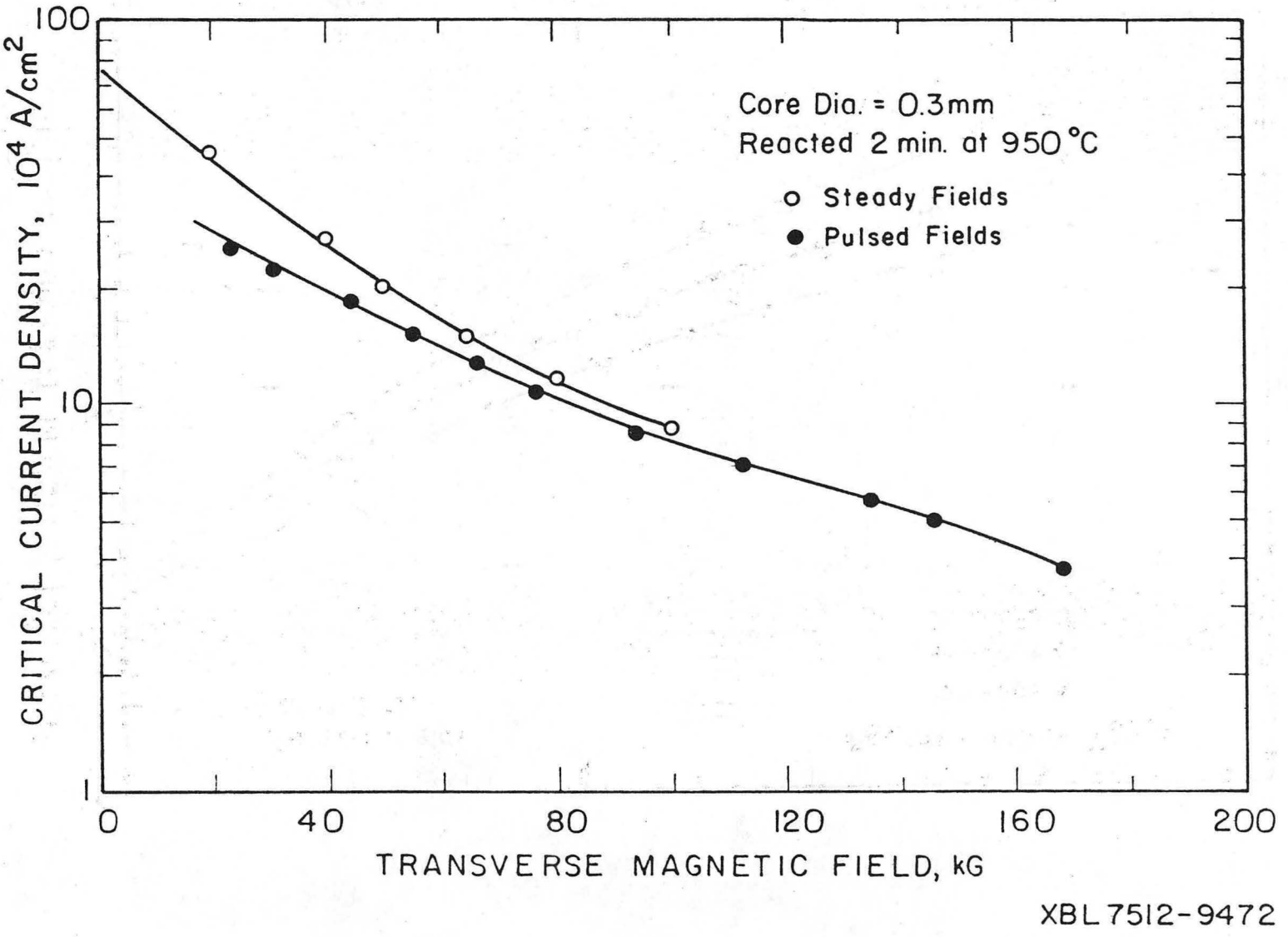

Fig. 21

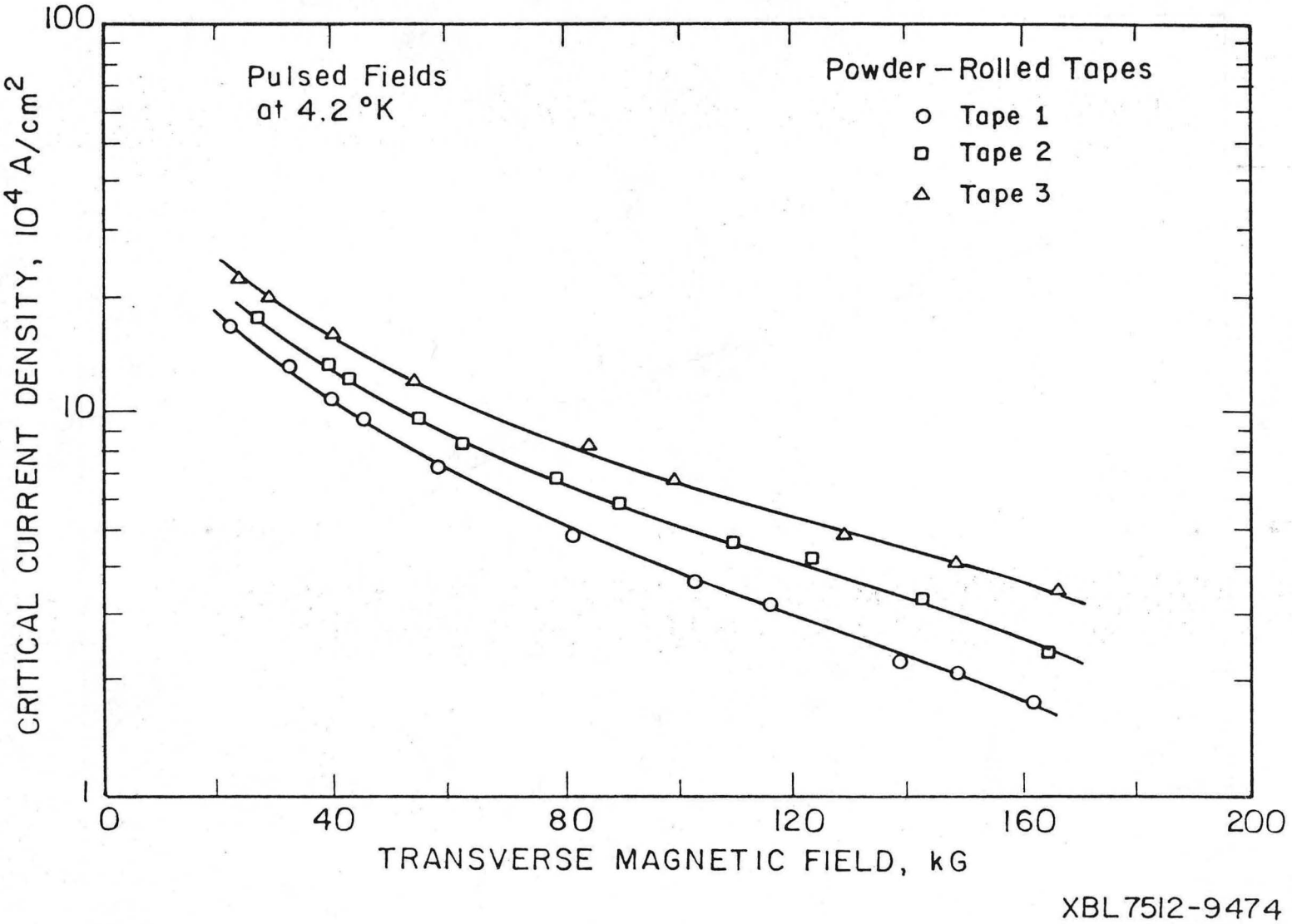
Pulsed Fields
at 4.2 °K
Powder – Rolled Tapes
Tape 1
Tape 2
Tape 3
CRITICAL CURRENT DENSITY, 10^4 A/cm^2
100
10
1
0
40
80
120
160
200
TRANSVERSE MAGNETIC FIELD, kG
XBL7512-9474

Fig. 22

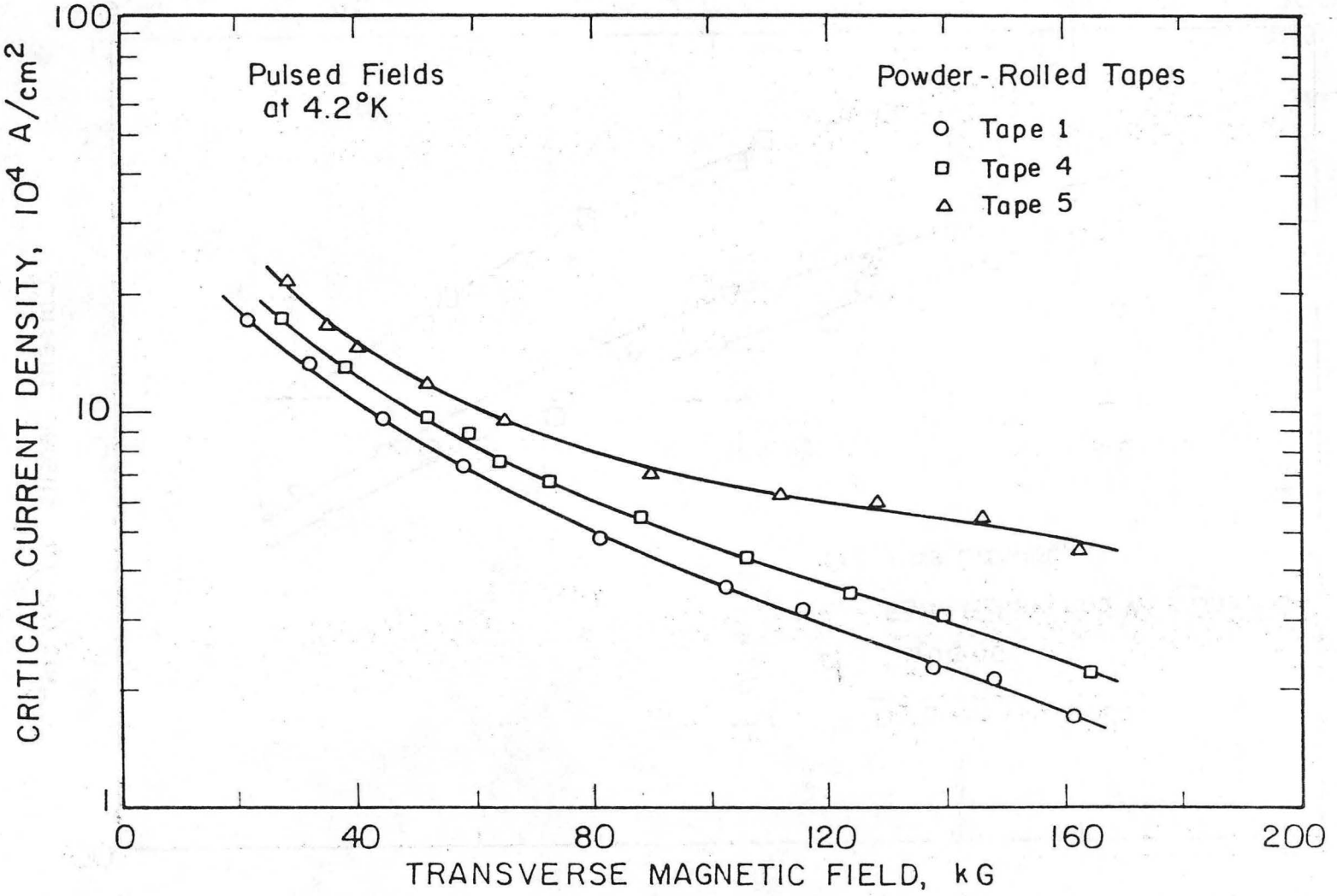

XBL 7512-9473

Fig. 23

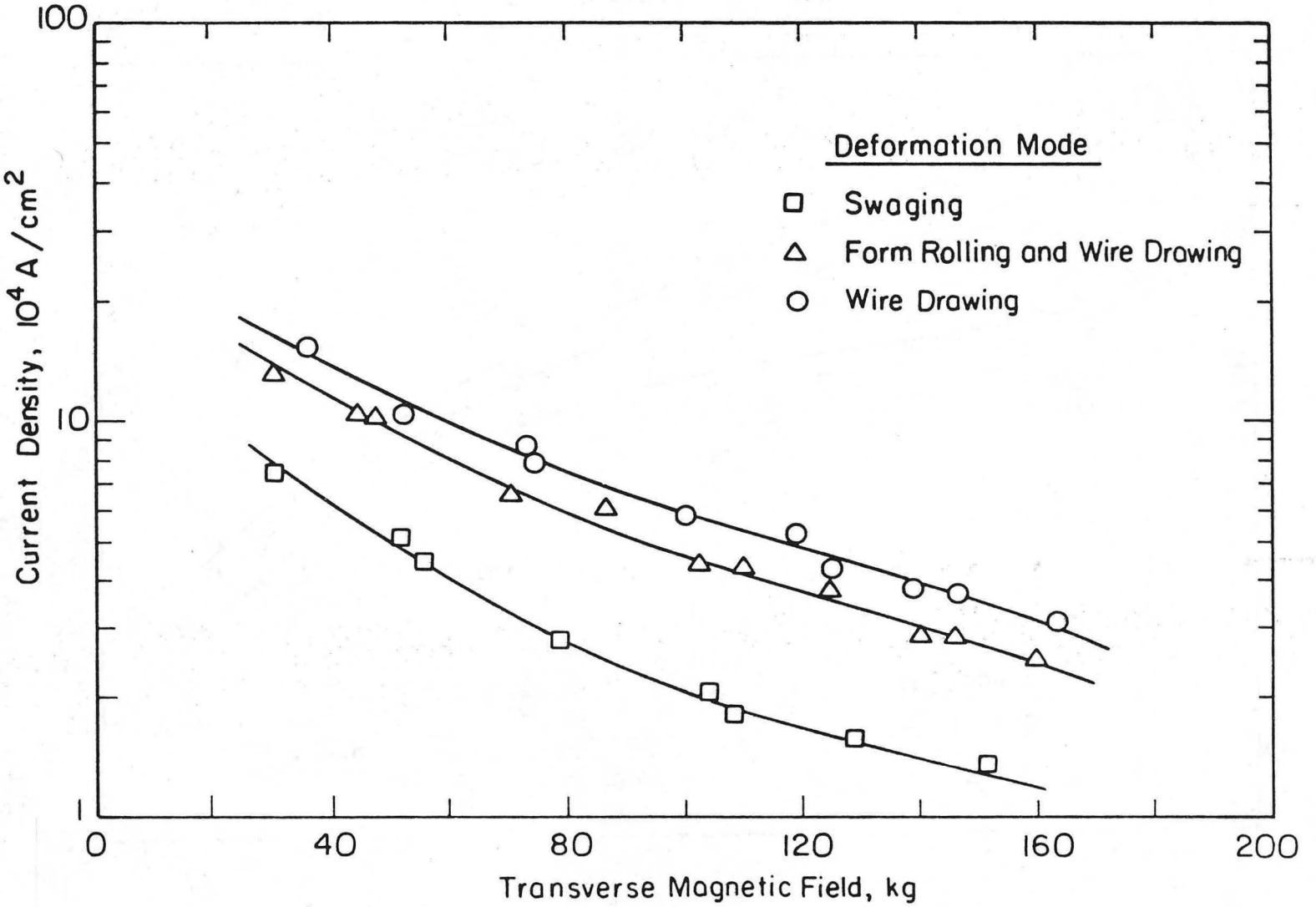

Fig. 24

XBL 7511-7570

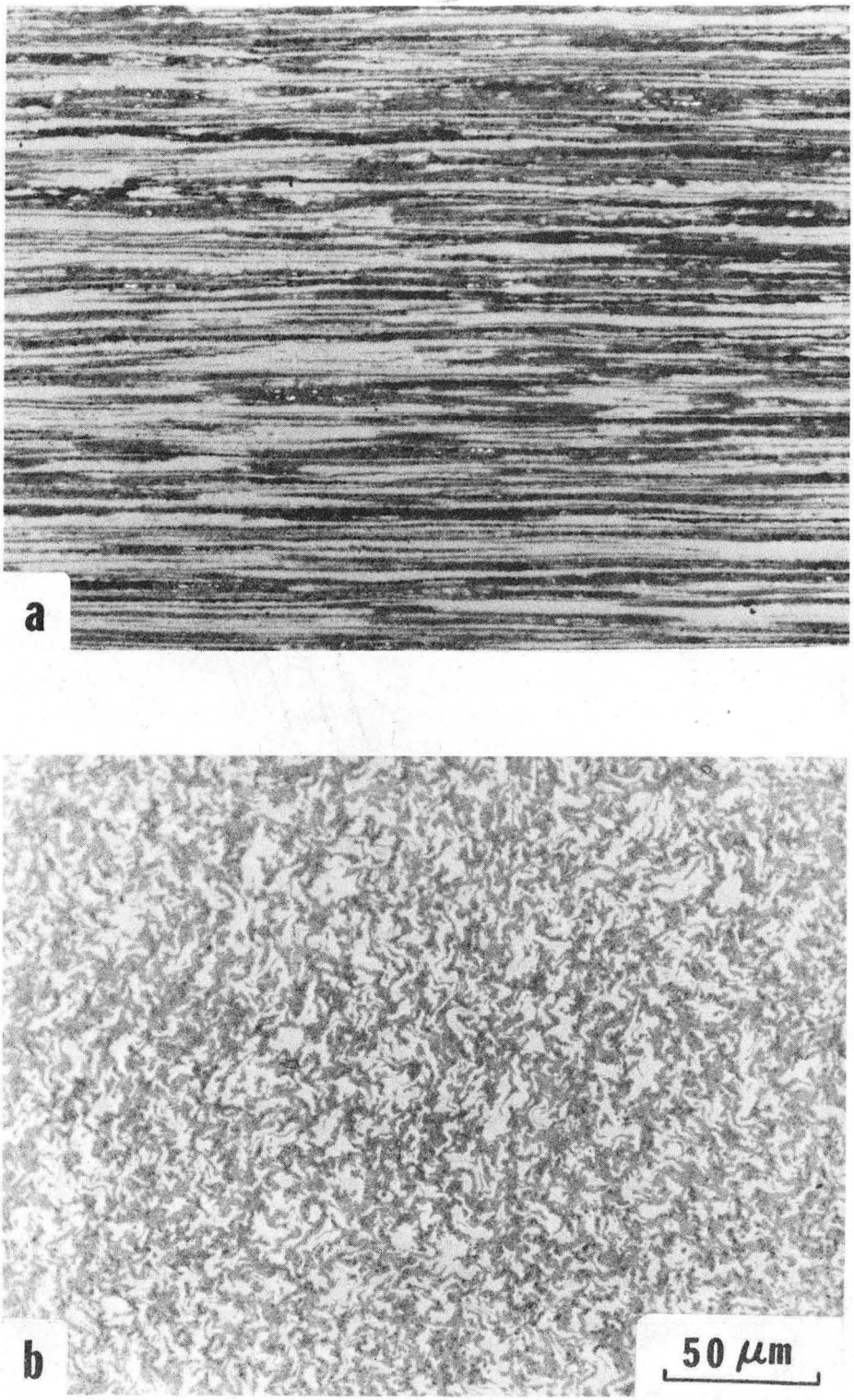

XBB 7512-9128

Fig. 25

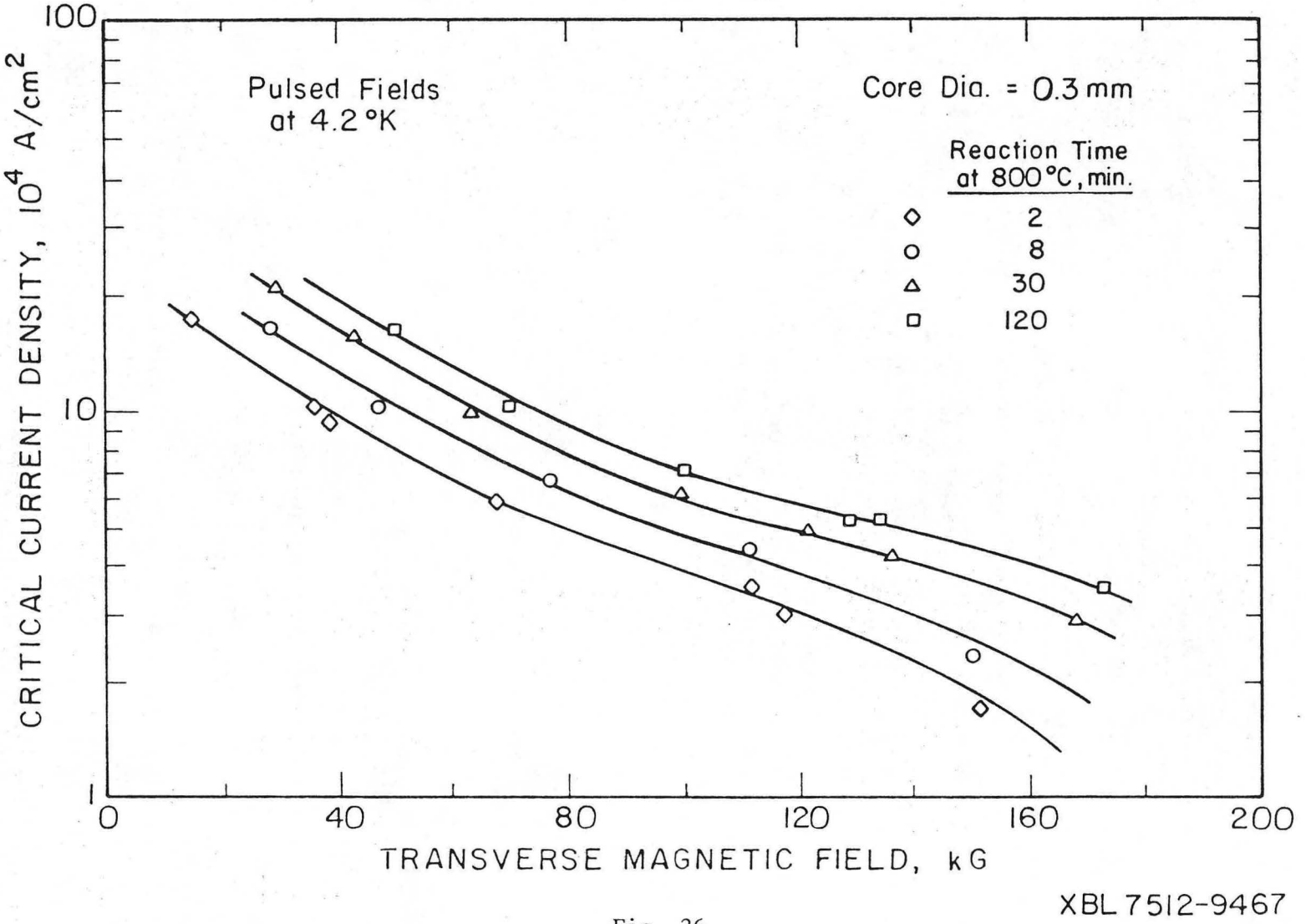
Pulsed Fields
at 4.2 °K
Core Dia. = 0.3 mm
Reaction Time
at 800 °C, min.
2
8
30
120
CRITICAL CURRENT DENSITY, 10^4 A/cm^2
100
10
1
0
40
80
120
160
200
TRANSVERSE MAGNETIC FIELD, kG
XBL 7512-9467

Fig. 26

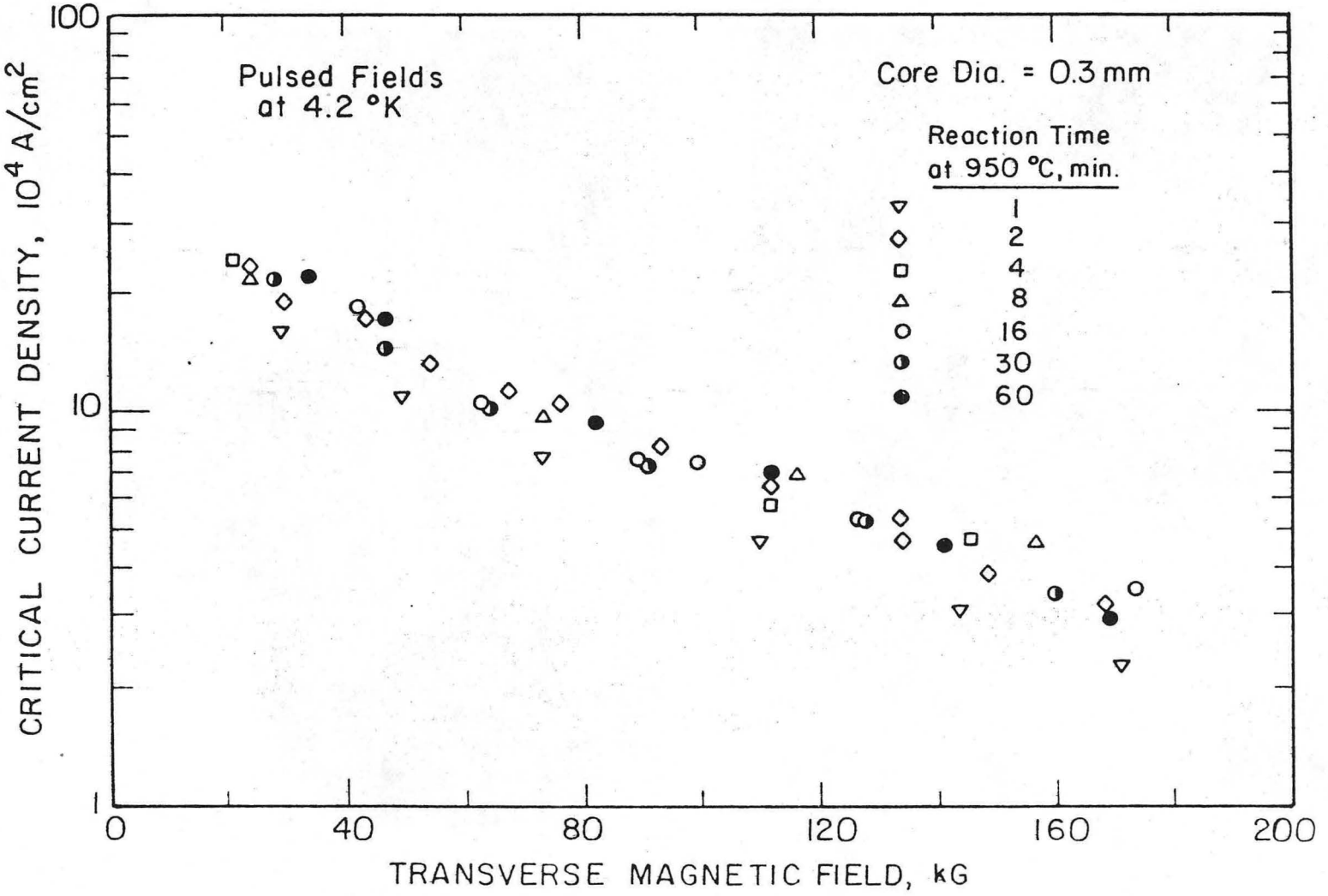

Fig. 27

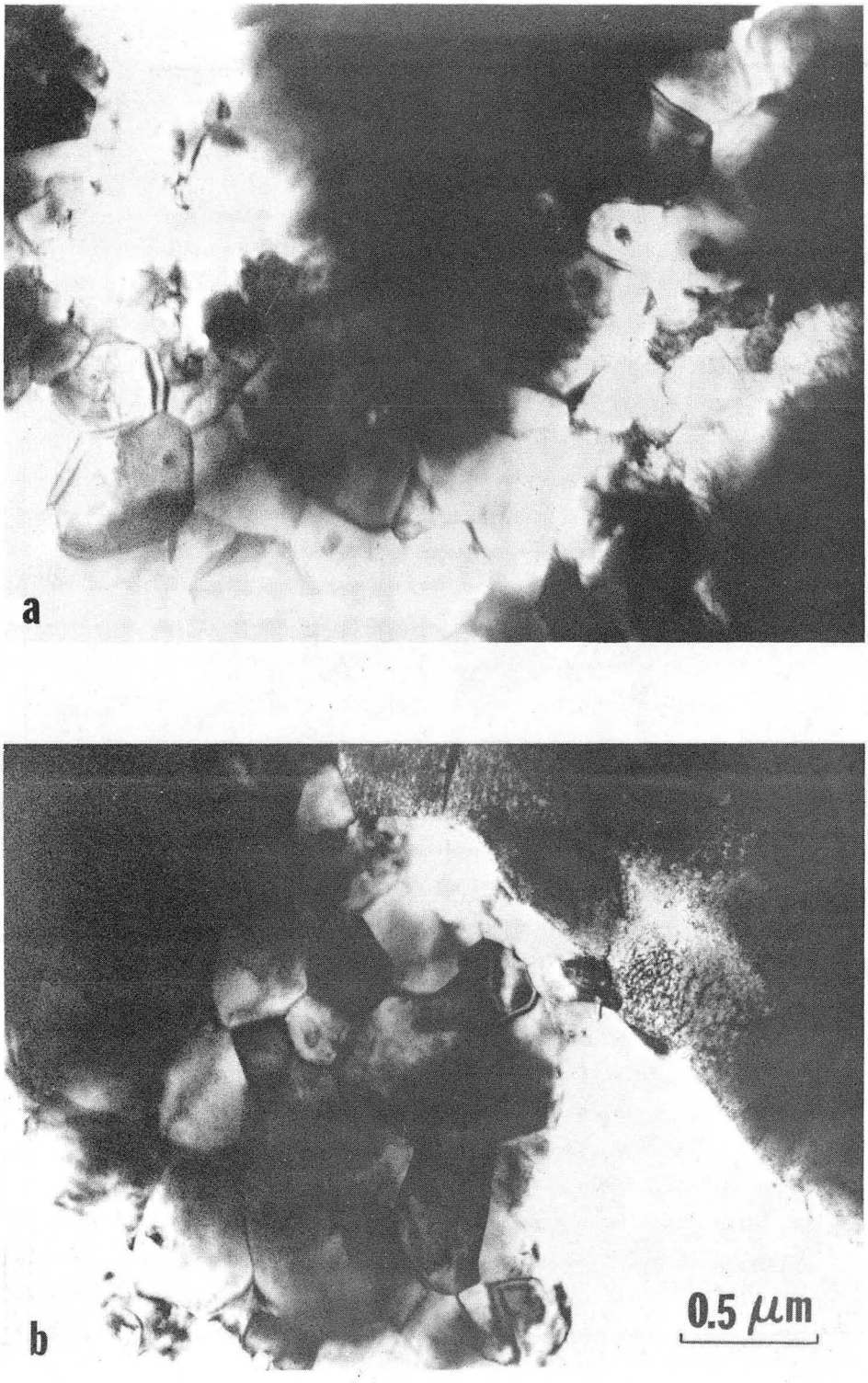

XBB 7512-9125

Fig. 28

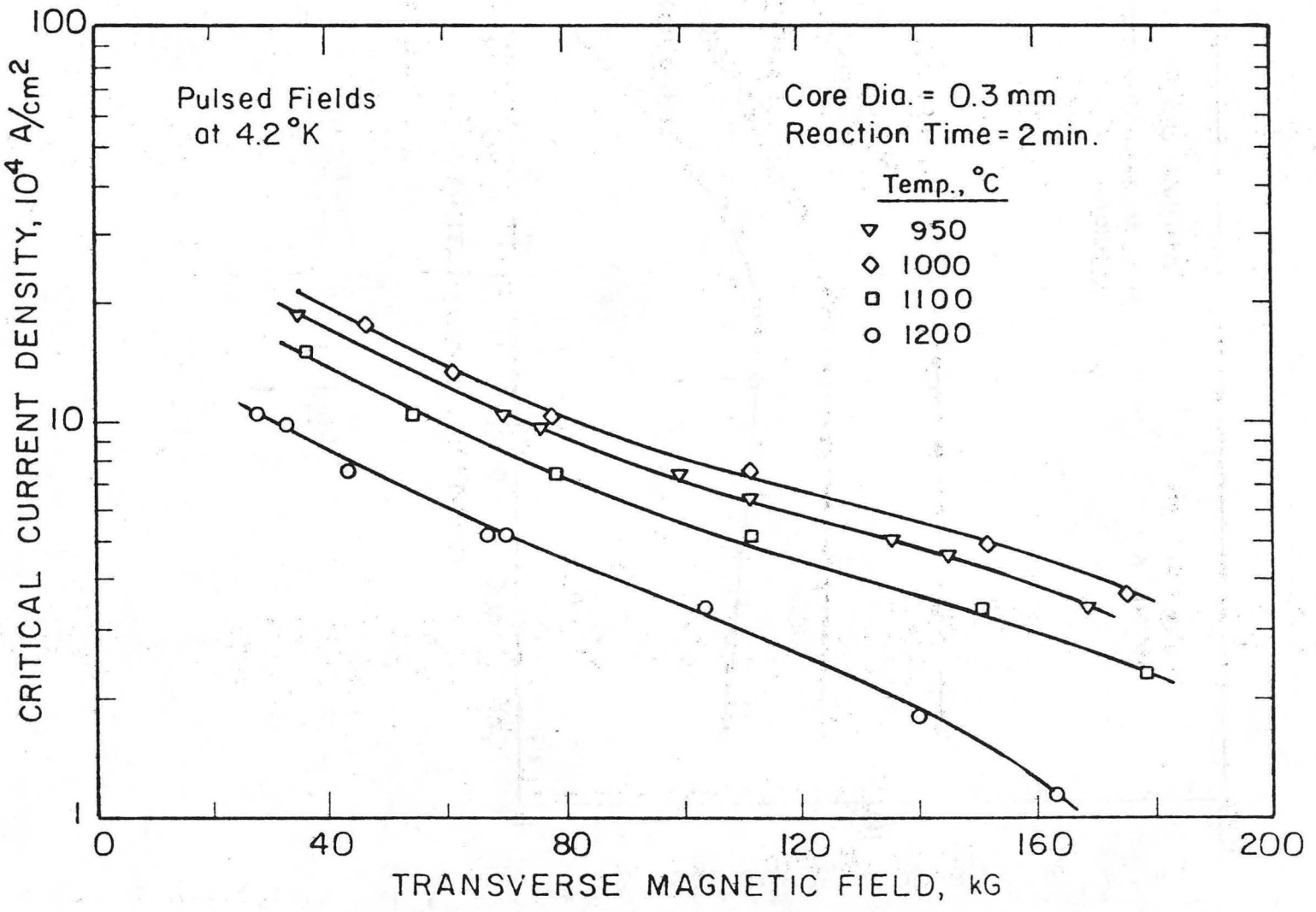

Fig. 29

XBL7512-9470

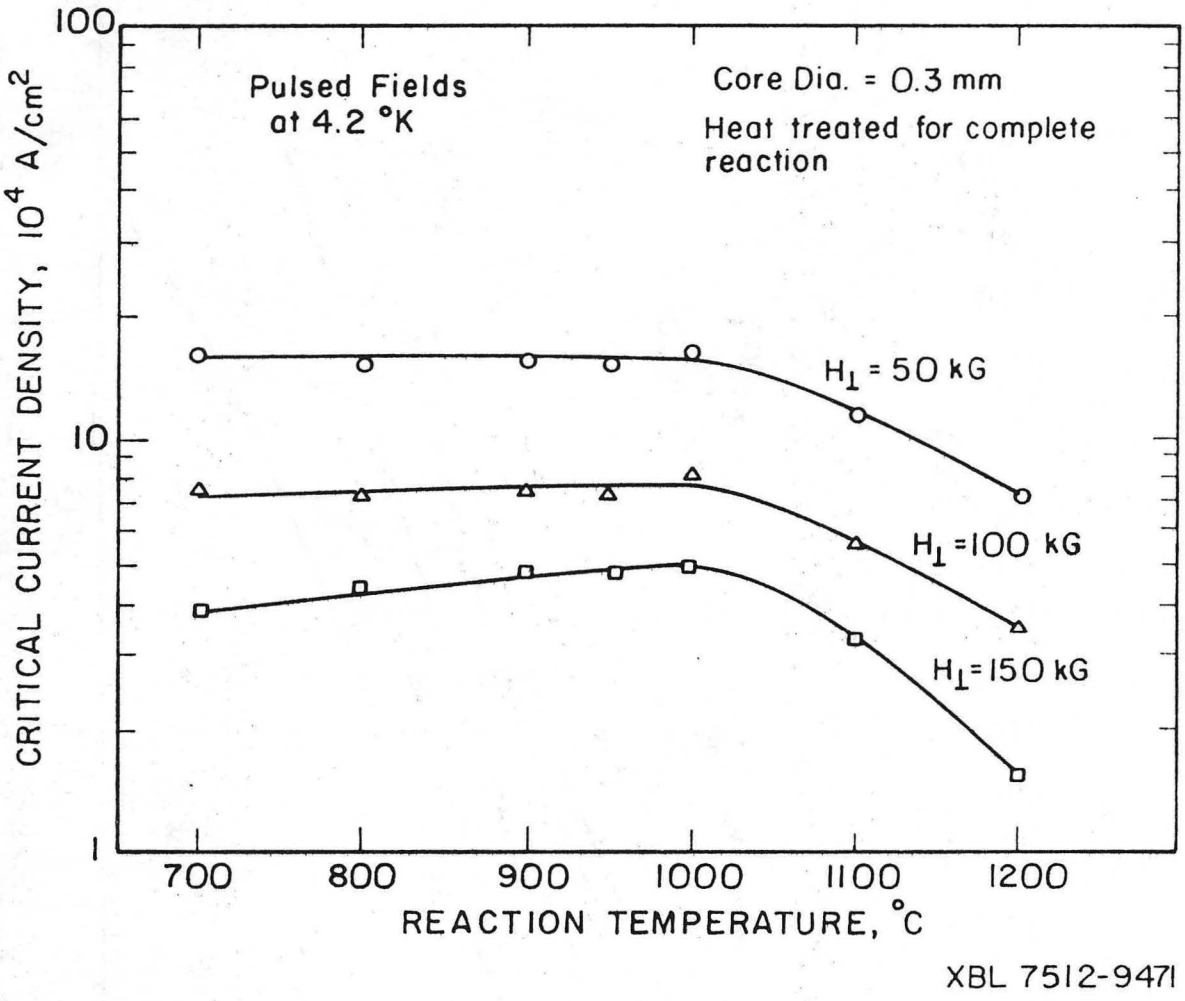
Pulsed Fields
at 4.2 °K
Core Dia. = 0.3 mm
Heat treated for complete
reaction
$H_\perp$ = 50 kG
$H_\perp$ =100 kG
$H_\perp$ =150 kG
CRITICAL CURRENT DENSITY, 10^4 A/cm^2
100
10
1
700
800
900
1000
1100
1200
REACTION TEMPERATURE, °C
XBL 7512-9471

Fig. 30

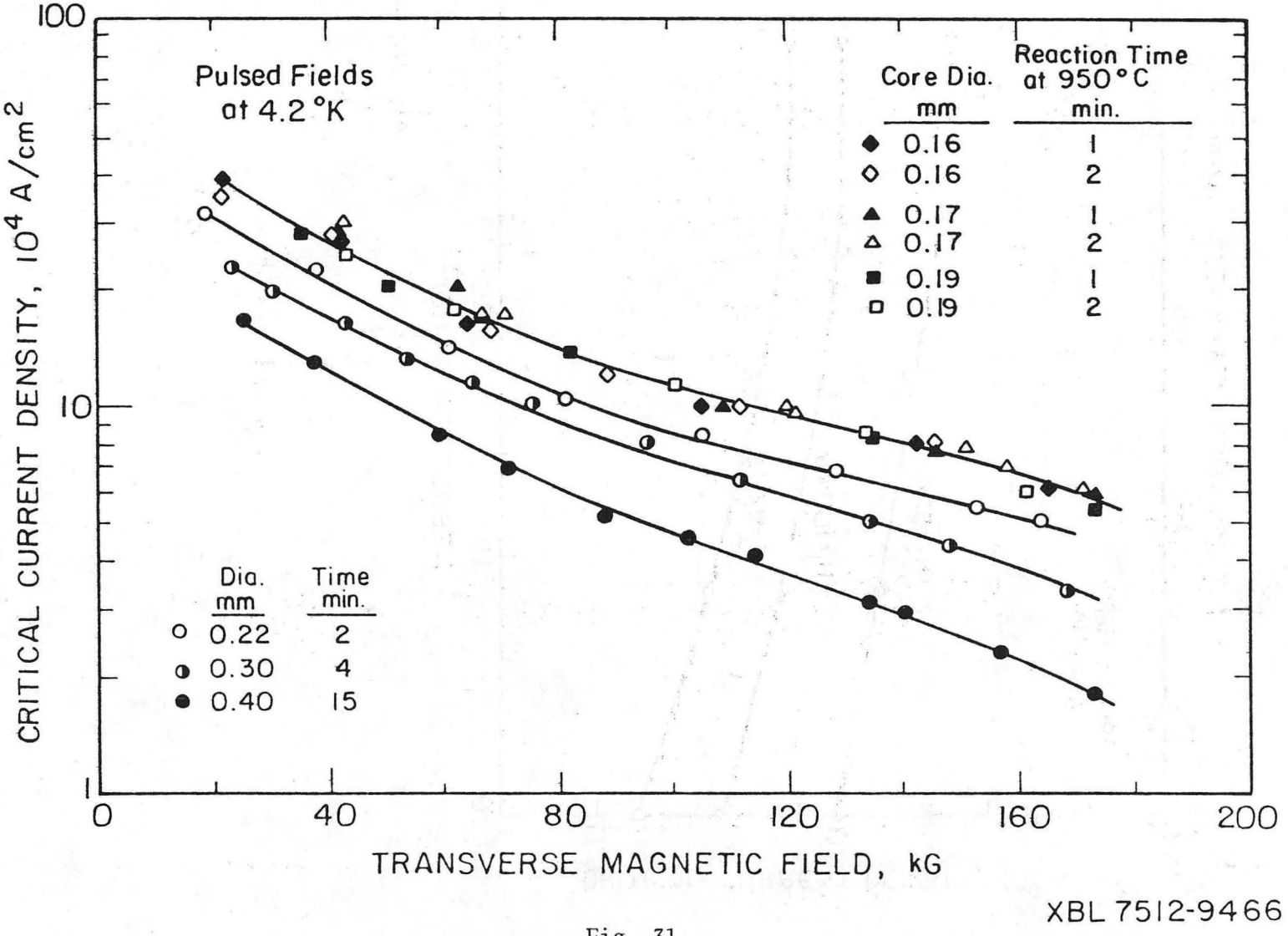

Fig. 31

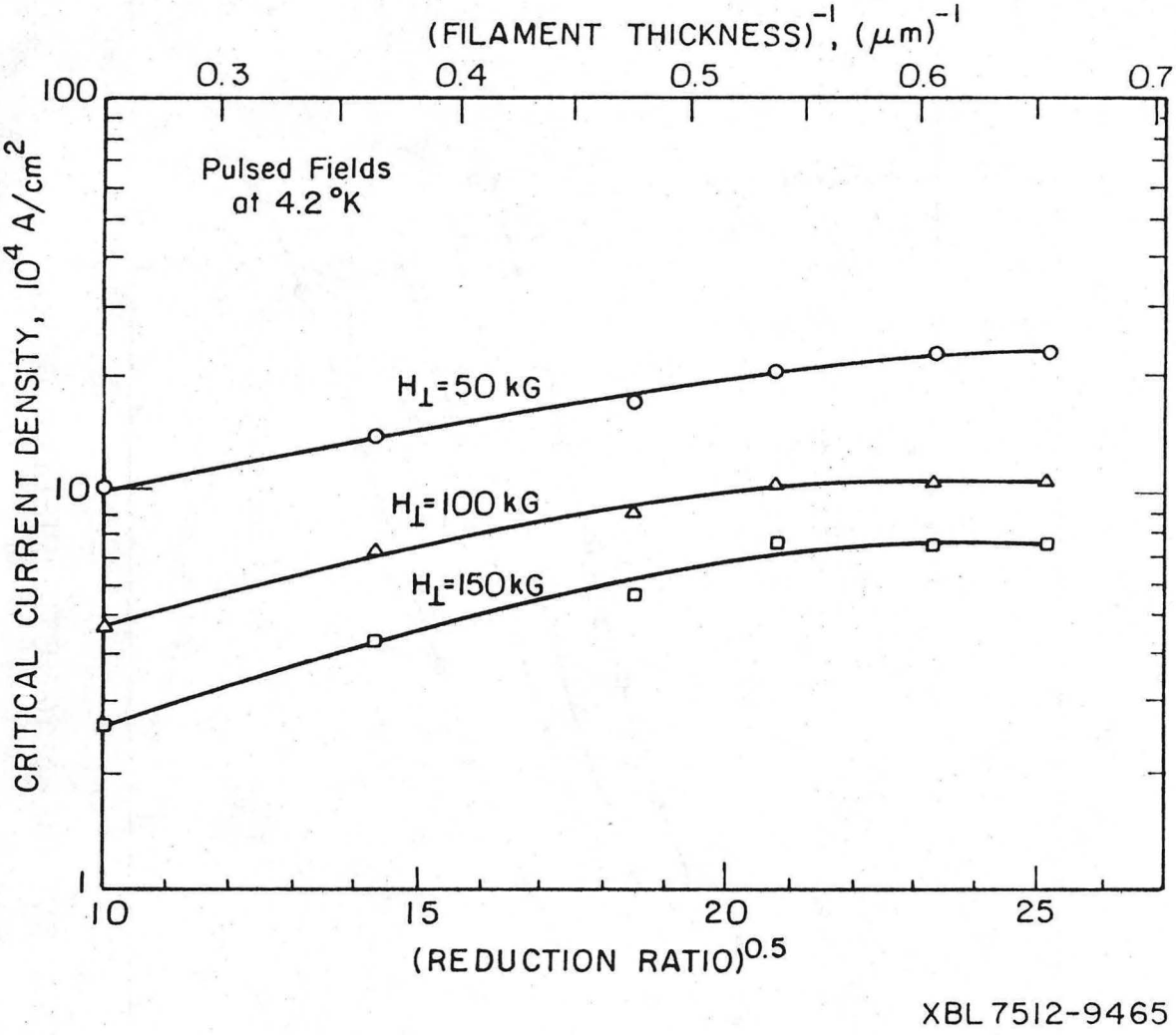
(FILAMENT THICKNESS)$^{-1}$, (μm)$^{-1}$
0.3
0.4
0.5
0.6
0.7
100
10
1
Pulsed Fields
at 4.2 °K
$H_\perp$=50 kG
$H_\perp$=100 kG
$H_\perp$=150kG
CRITICAL CURRENT DENSITY, 10^4 A/cm^2
10
15
20
25
(REDUCTION RATIO)$^{0.5}$
XBL 7512-9465

Fig. 32

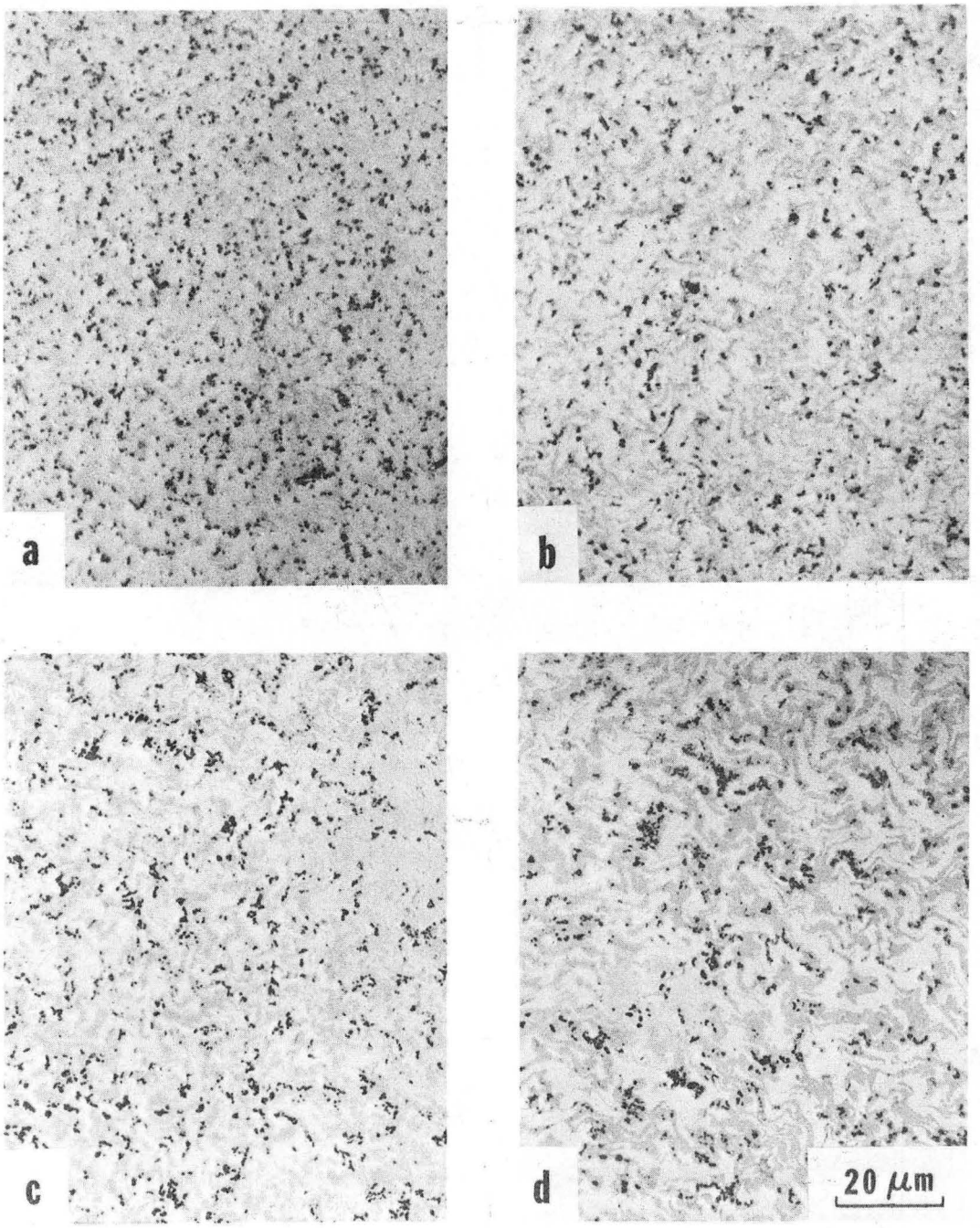

XBB 7512-9126

Fig. 33

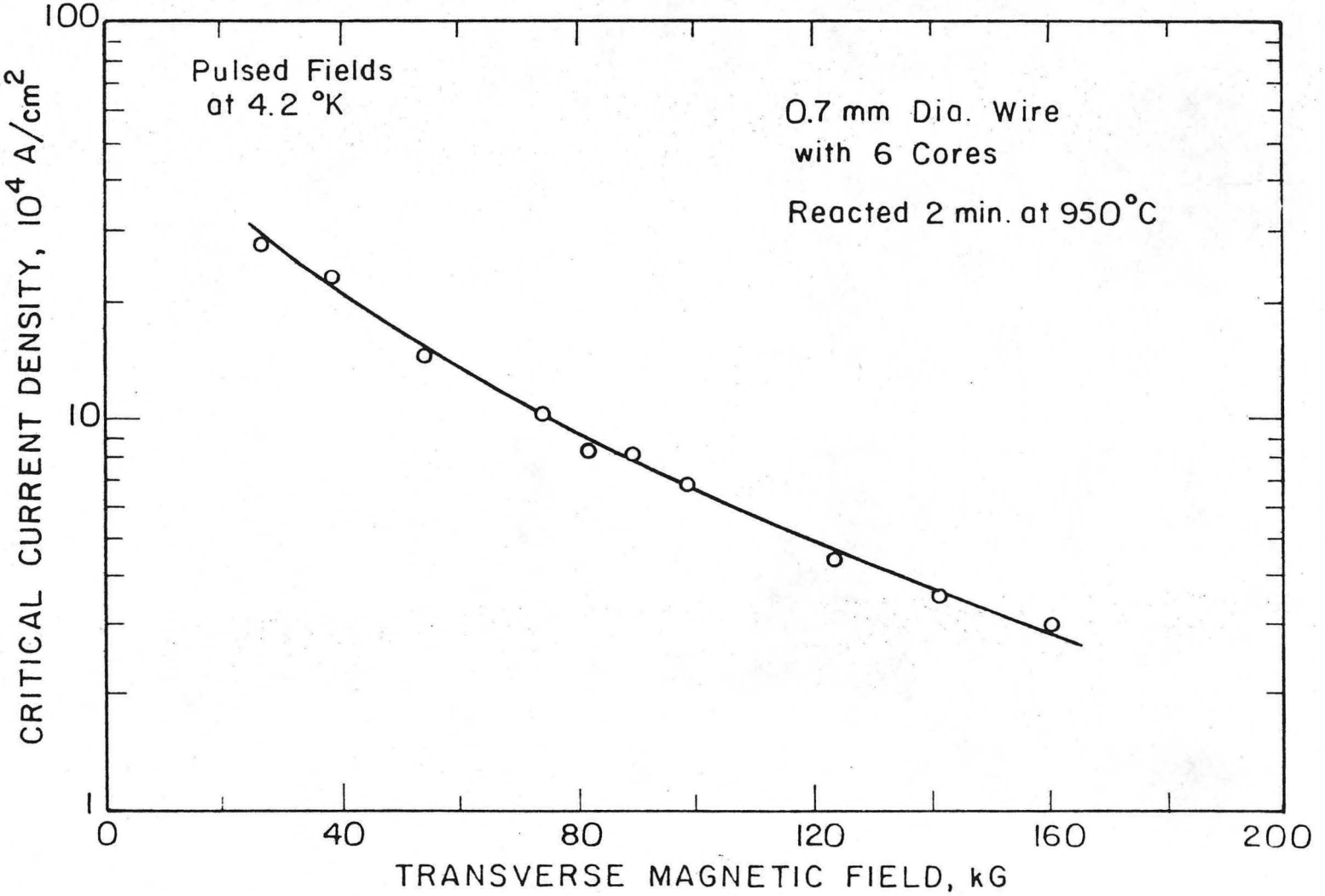

XBL 7512-9476

Fig. 34

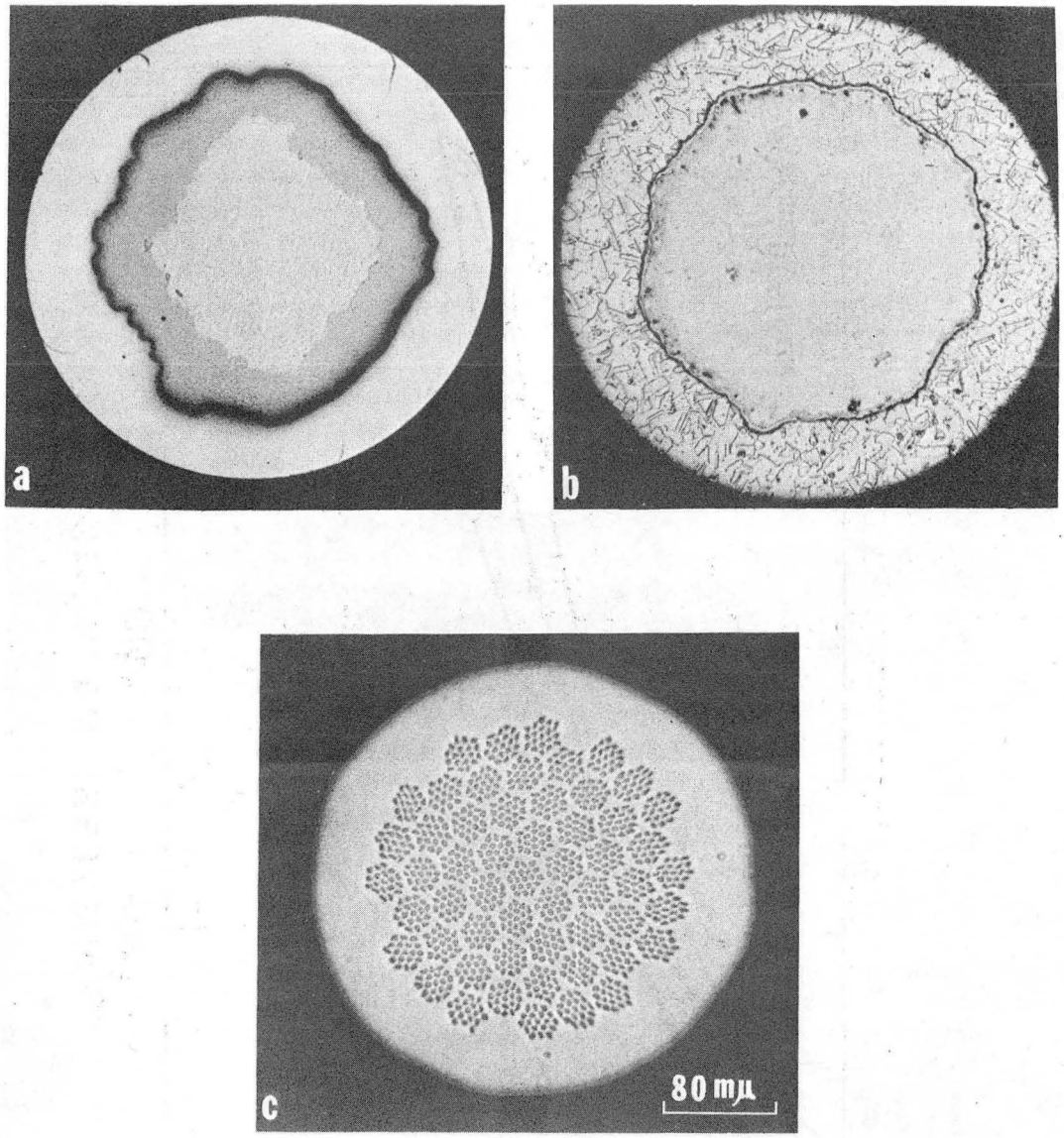

XBB 7512-9124

Fig. 35

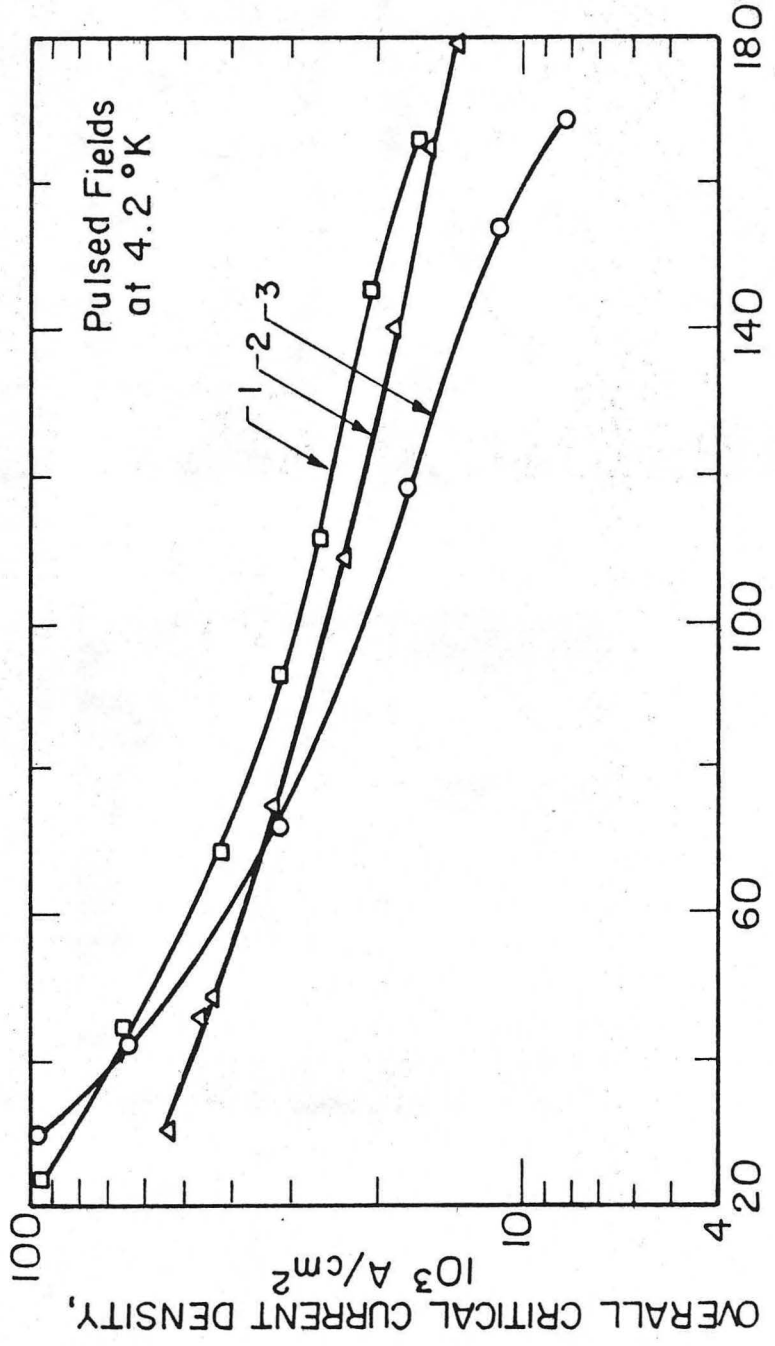
Pulsed Fields
at 4.2 °K
1
2
3
OVERALL CRITICAL CURRENT DENSITY,
10^3 A/cm^2
100
10
4
20
60
100
140
180
TRANSVERSE MAGNETIC FIELD, kG
XBL 7512-9468

Fig. 36

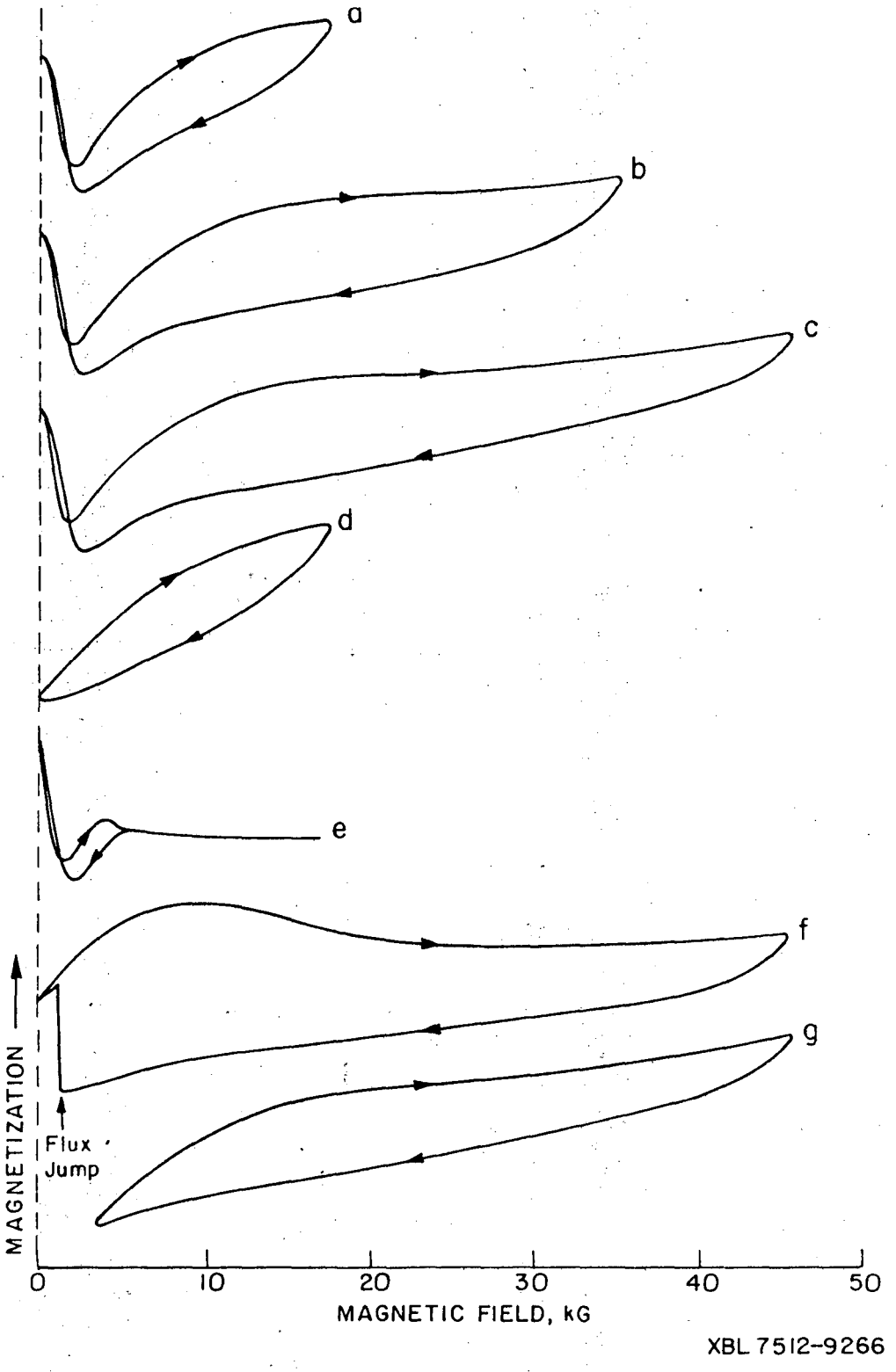

Fig. 37

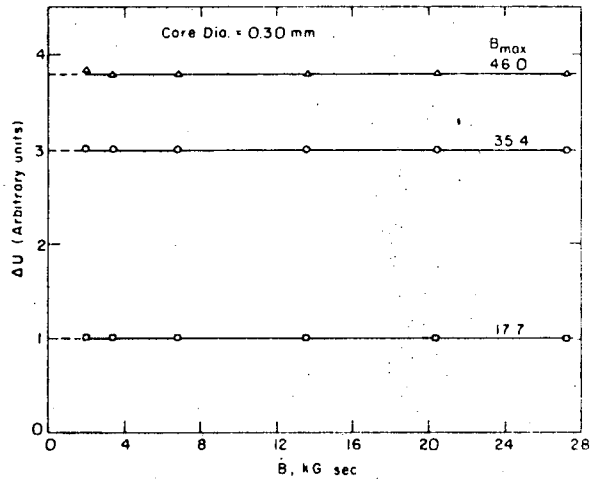
Core Dia. = 0.30 mm
B_{max}
46.0
35.4
17.7
ΔU (Arbitrary units)
0
1
2
3
4
0
4
8
12
16
20
24
28
Ḃ, kG sec

Fig. 38

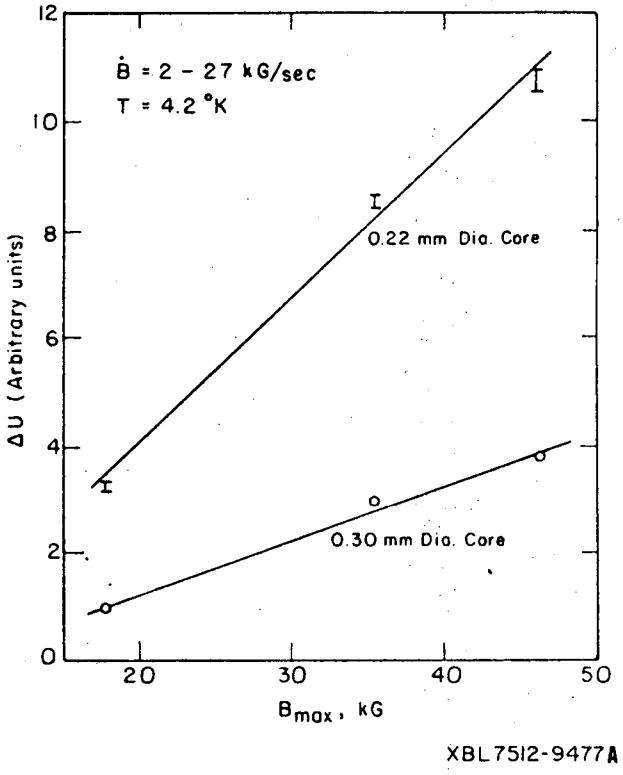
Ḃ = 2 - 27 kG/sec
T = 4.2 °K
0.22 mm Dia. Core
0.30 mm Dia. Core
ΔU (Arbitrary units)
0
2
4
6
8
10
12
20
30
40
50
B_{max}, kG
XBL7512-9477A

Fig. 39

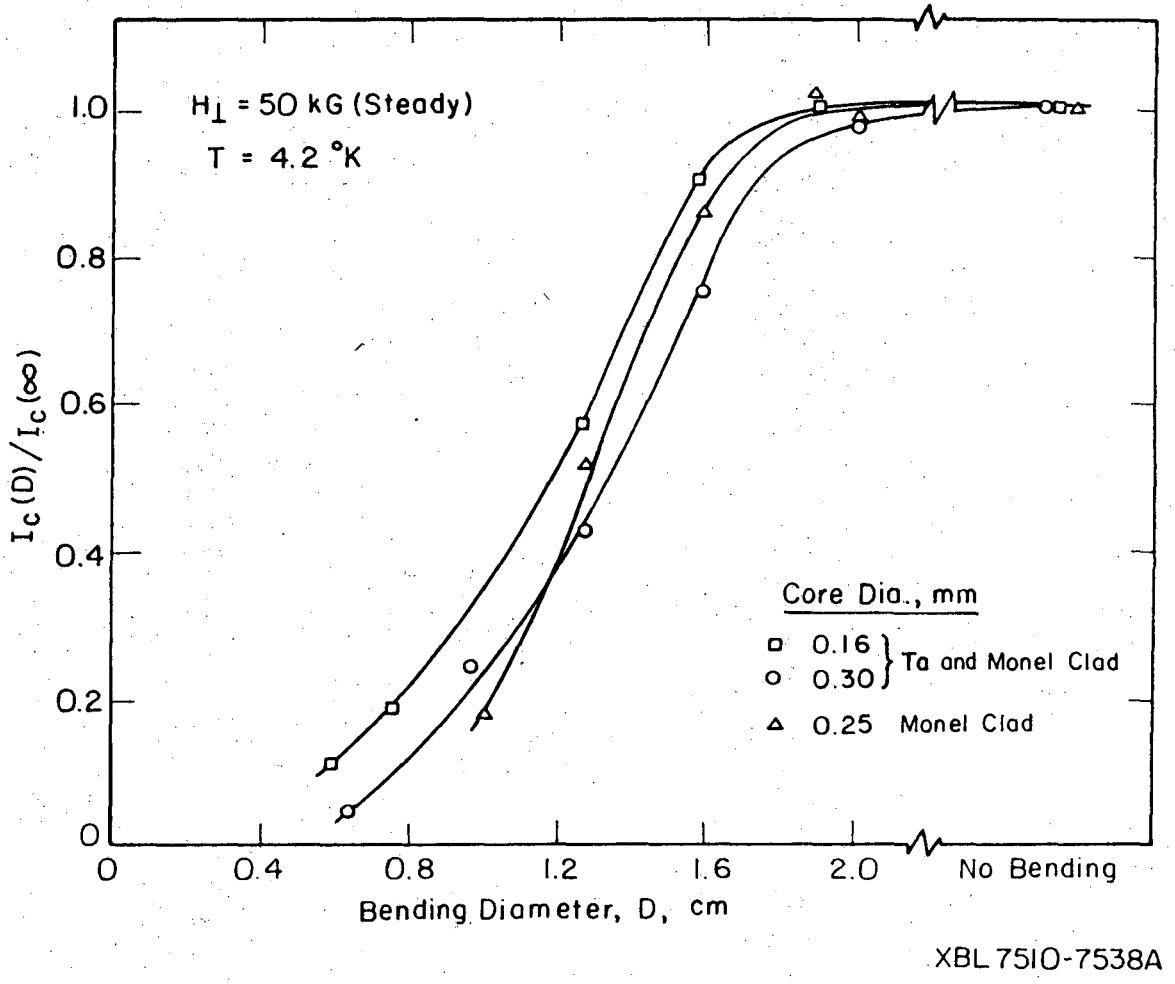

Fig. 40

TECHNICAL INFORMATION DIVISION
LAWRENCE BERKELEY LABORATORY
UNIVERSITY OF CALIFORNIA
BERKELEY, CALIFORNIA 94720